

AD-A120 848

LOW-LOSS FLEXIBLE DIELECTRIC WAVEGUIDE FOR
MILLIMETER-WAVE TRANSMISSION A. (U) CALIFORNIA INST OF
TECH PASADENA W B BRIDGES AUG 82 SRO-005-2
N00014-79-C-0839

1/1

UNCLASSIFIED

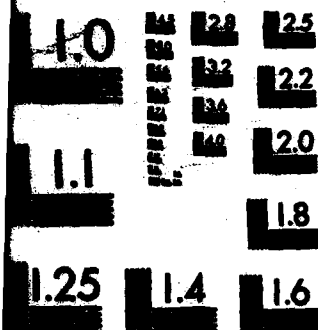
F/G 9/1

NL

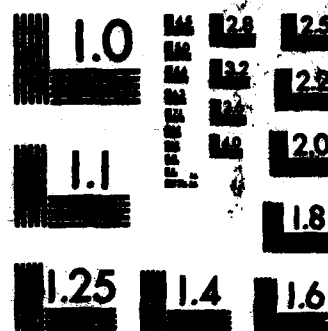
END

FORMED

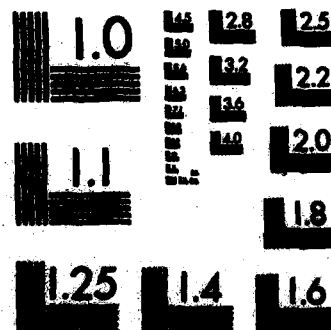
1/1



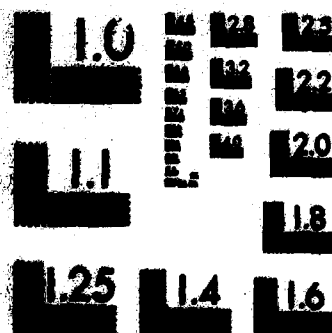
MICROCOPY RESOLUTION TEST CHART
NATIONAL BUREAU OF STANDARDS-1963-A



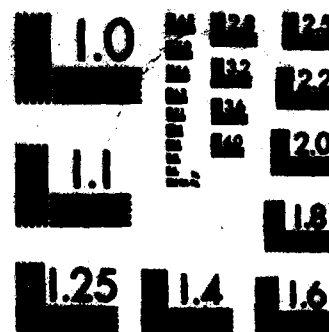
MICROCOPY RESOLUTION TEST CHART
NATIONAL BUREAU OF STANDARDS-1963-A



MICROCOPY RESOLUTION TEST CHART
NATIONAL BUREAU OF STANDARDS-1963-A



MICROCOPY RESOLUTION TEST CHART
NATIONAL BUREAU OF STANDARDS-1963-A



MICROCOPY RESOLUTION TEST CHART
NATIONAL BUREAU OF STANDARDS-1963-A

ADA 120848

CALIFORNIA INSTITUTE OF TECHNOLOGY

Pasadena, California



**Low Loss Flexible Dielectric Waveguide
for Millimeter-Wave Transmission
and its Application to Devices**

Annual Technical Report SRO-005-2

on

Contract N00014-79-C-0839

Project Number SRO-005

William B. Bridges - Principal Investigator

Reporting Period: 1 November 1980 - 28 February 1982

Prepared for Office of Naval Research, Code 427

Arlington VA 22217

Approved for Public Release

Reproduction, in whole or in part, is permitted for any purpose
of the U.S. Government

DTIC
S
OCT 29 1982
A

82 10 29 043

DTIC FILE COPY

UNCLASSIFIED

SECURITY CLASSIFICATION OF THIS PAGE (When Data Entered)

REPORT DOCUMENTATION PAGE		READ INSTRUCTIONS BEFORE COMPLETING FORM
1. REPORT NUMBER SRO-005-2	2. GOVT ACCESSION NO. AD A120 848	3. RECIPIENT'S CATALOG NUMBER
4. TITLE (and Subtitle) Low-Loss Flexible Dielectric Waveguide for Millimeter-Wave Transmission and its Application to Devices		5. TYPE OF REPORT & PERIOD COVERED Annual Technical 11/1/80 - 2/28/82
7. AUTHOR(s) William B. Bridges		6. PERFORMING ORG. REPORT NUMBER ONR 82-1-ONE
9. PERFORMING ORGANIZATION NAME AND ADDRESS California Institute of Technology, 128-95 Pasadena, California 91125		8. CONTRACT OR GRANT NUMBER(s) N00014-79-C-0839
11. CONTROLLING OFFICE NAME AND ADDRESS Office of Naval Research Code 427 Arlington, VA 22217		10. PROGRAM ELEMENT, PROJECT, TASK AREA & WORK UNIT NUMBERS 61153N RR 021-02-03
14. MONITORING AGENCY NAME & ADDRESS (if different from Controlling Office)		12. REPORT DATE August 1982
		13. NUMBER OF PAGES 44
		15. SECURITY CLASS. (of this report) UNCLASSIFIED
		15a. DECLASSIFICATION/DOWNGRADING SCHEDULE
16. DISTRIBUTION STATEMENT (of this Report) Approved for public release; distribution unlimited.		
17. DISTRIBUTION STATEMENT (of the abstract entered in Block 20, if different from Report)		
18. SUPPLEMENTARY NOTES ONR Scientific Officer: Tel. (202) 696-4218		
19. KEY WORDS (Continue on reverse side if necessary and identify by block number)		
millimeter-waves	KRS-5	phase shifter
dielectric waveguides	KRS-6	electro-optics
dielectric loss	finite difference method	LiNbO ₃
dielectric constant	finite element method	
loss tangent	nonlinear effects	
20. ABSTRACT (Continue on reverse side if necessary and identify by block number)		
<p>A finite-difference method has been developed for computing the propagation constants and field distributions for dielectric waveguides of arbitrary cross section and dielectric constant. The results of the method are compared with the exact solution for a round waveguide. Additional calculations are made for rectangular waveguides and the results compared with Marcattili's approximate solutions.</p> <p>Results are given for a dielectric waveguide phase shifter using a</p>		

DD FORM 1 JAN 73 1473

EDITION OF 1 NOV 68 IS OBSOLETE
S/N 0102-LP-014-6601

UNCLASSIFIED

SECURITY CLASSIFICATION OF THIS PAGE (When Data Entered)

UNCLASSIFIED

SECURITY CLASSIFICATION OF THIS PAGE (When Data Entered)

LiNbO₃ waveguide. Approximately one radian of phase shift at 94 GHz was obtained with 1000 V peak audio frequency voltage applied to electrodes on the LiNbO₃ waveguide. Amplitude modulation of 70% was observed in a microwave bridge configuration, in good agreement with theory. Other uses of nonlinear/electro-optic materials in the millimeter wave range are discussed, including electronically-scanned antennas and electronically-tuned filters.

Accession For	
NTIS GR&I	<input checked="checked" type="checkbox"/>
DTIC TAB	<input type="checkbox"/>
Unannounced	<input type="checkbox"/>
Justification	
In	
Distribution	
Availability	
Dist	
A	



UNCLASSIFIED

SECURITY CLASSIFICATION OF THIS PAGE (When Data Entered)

CALIFORNIA INSTITUTE OF TECHNOLOGY

Pasadena, California



**Low Loss Flexible Dielectric Waveguide
for Millimeter-Wave Transmission
and its Application to Devices**

Annual Technical Report SRO-005-2

on

Contract N00014-79-C-0839

Project Number SRO-005

William B. Bridges - Principal Investigator

Reporting Period: 1 November 1980 - 28 February 1982

Prepared for Office of Naval Research, Code 427

Arlington VA 22217

Approved for Public Release

**Reproduction, in whole or in part, is permitted for any purpose
of the U.S. Government**

This report covers research performed under contract N00014-79-C-0839 at the California Institute of Technology, Pasadena, California 91125 and, under subcontract, at the Hughes Research Laboratories, Malibu, California 90265 for the second year of this three year program, 1 November 1980 through 28 February 1982.

Personnel contributing to this work were:

William B. Bridges, Professor of Electrical Engineering and Applied Physics, Caltech; Principal Investigator (213) 356-4809.

Marvin B. Klein, Member of the Technical Staff, Hughes Research Labs.,

Co-principal Investigator (213) 456-6411, x247.

Edgard Schweig, Graduate Student,* Caltech (213) 356-4854.

The authors of each section of the report are identified at the beginning of the section.

*Present address: Av. Bolivia, 971, Breña, Lima, Peru.

TABLE OF CONTENTS

I.	INTRODUCTION AND SUMMARY	I-1
II.	COMPUTER ANALYSIS OF RECTANGULAR DIELECTRIC WAVEGUIDE	II-1
III.	ELECTRO-OPTIC DEVICES IN DIELECTRIC WAVEGUIDE . . .	III-1

I. INTRODUCTION AND SUMMARY (W. B. Bridges)

A. Summary and Results

During the second year of this contract to study dielectric waveguides, two major tasks were pursued. First, a method of computing the propagation constants and the field distributions for the modes of dielectric waveguides of arbitrary cross section and arbitrary dielectric constant was developed, based on the method of finite differences. This technique was applied to a round dielectric waveguide so that a comparison could be made with a case for which a rigorous exact solution is known. The technique was also applied to rectangular and square waveguides and compared with the approximate solutions of Marcatili and others. A brief description of the method and some of the results are given in Section II of this report. More details appear elsewhere (see Section C below).

The second major task undertaken this year was the examination of the feasibility of using nonlinear or electro-optic materials in dielectric waveguide form to realize useful functions. As a specific example of such a component, an electro-optic phase shifter was constructed using a lithium niobate (LiNbO_3) waveguide. Low frequency voltages applied to electrodes forming a portion of the waveguide structure induced phase shifts in the 94 GHz signal propagating along the waveguide. Approximately one radian of phase shift could be obtained with applied electric fields well below the breakdown value for the LiNbO_3 dielectric. Other components, such as electronically scanned antennas and electronically tuned filters were considered, and some insights were developed for the future of materials requirements for such applications.

B. Future Plans

The development of the finite difference method is now felt to be sufficiently complete for our use. In the future we may calculate cases of

special interest to us, but we plan no further development of the theory itself at this time.

Work will continue on the application of nonlinear materials to millimeter wave dielectric devices as outlined in Section III of this report. This work will benefit by coordination with other, separately funded programs at the Hughes Research Laboratories, through the end of the subcontract period, 31 August 1982.

We plan to return to the question of surface wave propagation along lossy dielectrics as a possible explanation of the low attenuations actually observed in KRS-5 fibers, losses much lower than that predicted for the HE_{11} mode with the measured loss tangent at 94 GHz. (These puzzling results were described in more detail in our previous annual report.) While the waveguide attenuation actually measured for KRS-5 was of the order of 20 dB/meter, too large to be practical for most applications, we feel it is important scientifically to resolve this enigma.

A new approach to the problem of realizing a flexible dielectric waveguide was considered near the end of the period covered by this report, and we are now actively pursuing it. Low loss, high dielectric constant materials are available for the millimeter wave range, but they are all rigid materials (for example, Alumina, GaAs, Silicon). We are now considering the use of these materials in finely powdered form, contained in a thin, flexible polymer jacket (e.g., Teflon). Preliminary measurements of such powders are now being carried out at 10 GHz to determine the relation of dielectric constant and loss tangent of the powder form to the bulk form. If these prove to be successful, then flexible waveguides will be fabricated for test. (We must know the dielectric constant of the packed powder before we can design a reasonable guide.) These measurements will then be extended to 94 GHz as soon as possible. While the primary intent of this work is to provide a flexible

dielectric waveguide medium, if successful, it could also impact the ease of fabrication of rigid dielectric components as well. One can imagine a complicated configuration of directional couplers, filters, etc., fabricated by filling the voids in a thin vacuum-formed plastic sheet (similar to "bubble-pack"). Such an assembly could stand alone as true dielectric waveguide, or be capped with a metal plate to form image guide. We intend to pursue these ideas as well, if the basic measurements on powders prove successful.

C. Publications and Presentations

The following papers were given at the Sixth International Conference of Infrared and Millimeter Waves in Miami, December 1981:

1. "Measurement of the Dielectric Constant and Loss Tangent of Thallium Mixed Halide Crystals KRS-5 and KRS-6 at 95 GHz", W. B. Bridges, M. B. Klein, and E. Schweig.
2. "Computer Analysis of Rectangular Dielectric Waveguide for Millimeter Waves", E. Schweig and W. B. Bridges.
3. "Electro-Optic Devices in Dielectric Waveguide", M. B. Klein.

The following papers have appeared or have been submitted for publication:

1. W. B. Bridges, M. B. Klein, and E. Schweig, "Measurement of the Dielectric Constant and Loss Tangent of Thallium Mixed Halide Crystals KRS-5 and KRS-6 at 95 HGz", IEEE Trans. on Microwave Theory and Techniques, Vol. MTT-30, pp. 286-292, March 1982.
2. E. Schweig, "Dielectric Waveguides for Millimeter Waves," Ph.D. Thesis, California Institute of Technology, June 1982.
3. E. Schweig and W. B. Bridges, "Computer Analysis of Dielectric Waveguides: A Finite-Difference Method", submitted to IEEE Trans. on Microwave Theory and Techniques.

to read: "H. B. Klein, 'Electric Discharge Apparatus at 95 GHz Using'

1950, submitted to the International Journal of Infrared and Mill-

imeter Waves.

Following the review in this journal, the author was notified to

submit a revised manuscript. The author's response was that the

manuscript was not suitable for publication in this journal.

The author's response was that the manuscript was not suitable for

References and Bibliography

The author's manuscript was given a thorough review and was

found to be of high quality and suitable for publication.

The author's manuscript was given a thorough review and was

found to be of high quality and suitable for publication.

The author's manuscript was given a thorough review and was

found to be of high quality and suitable for publication.

The author's manuscript was given a thorough review and was

found to be of high quality and suitable for publication.

The following papers were referred to have been submitted for publication:

1. H. B. Klein, "Electric Discharge Apparatus at 95 GHz Using"

2. H. B. Klein, "Electric Discharge Apparatus at 95 GHz Using"

3. H. B. Klein, "Electric Discharge Apparatus at 95 GHz Using"

4. H. B. Klein, "Electric Discharge Apparatus at 95 GHz Using"

5. H. B. Klein, "Electric Discharge Apparatus at 95 GHz Using"

6. H. B. Klein, "Electric Discharge Apparatus at 95 GHz Using"

7. H. B. Klein, "Electric Discharge Apparatus at 95 GHz Using"

8. H. B. Klein, "Electric Discharge Apparatus at 95 GHz Using"

9. H. B. Klein, "Electric Discharge Apparatus at 95 GHz Using"

II. COMPUTER ANALYSIS OF RECTANGULAR DIELECTRIC WAVEGUIDES (E. Schweig)

A. Introduction

Image guides made of rectangular high permittivity dielectric material have been suggested as a practical waveguiding structure for use in millimeter-wave integrated circuits (MMIC) [Refs. II-1, II-2]. The use of a high-resistivity semiconductor material is particularly interesting since the possibility that active devices may be fabricated directly into the transmission line can be considered.

Rectangular dielectric waveguides for integrated optical circuits have been investigated analytically by Marcatili [Ref. II-3]. Several other workers--Knox and Toullos [Ref. II-1], Solbach [Ref. II-4] and Yeh [Ref. II-5] among others--have developed techniques for analyzing rectangular dielectric guides. Some of these methods are limited to weakly-guiding optical waveguides (small index ratio), or impose geometric conditions that are insufficiently general for our purposes. We also have investigated the analysis of such dielectric waveguides and found that the approximations introduced by Marcatili [Ref. II-3] are not valid when the permittivity of the guide is high compared to the outer medium ($\epsilon_{\text{guide}}/\epsilon_{\text{clad}} \sim 10$). We propose instead a numerical method based on finite-differences for computing accurate propagation characteristics and field distributions.

B. Description of the Problem

A rectangular dielectric waveguide of relative permittivity K_1 , surrounded by an infinite medium of relative permittivity K_0 is the basic element that we consider for our theoretical investigations (Fig. II-1a). In practice, the guide is often supported by a dielectric of much lower permittivity K_2 (Fig. II-1b) or by a metal plane (Fig. II-1c). In first approximation, we can neglect the influence of the dielectric support if the modes are well guided within the rectangular core. The effect of the metal plane is to allow

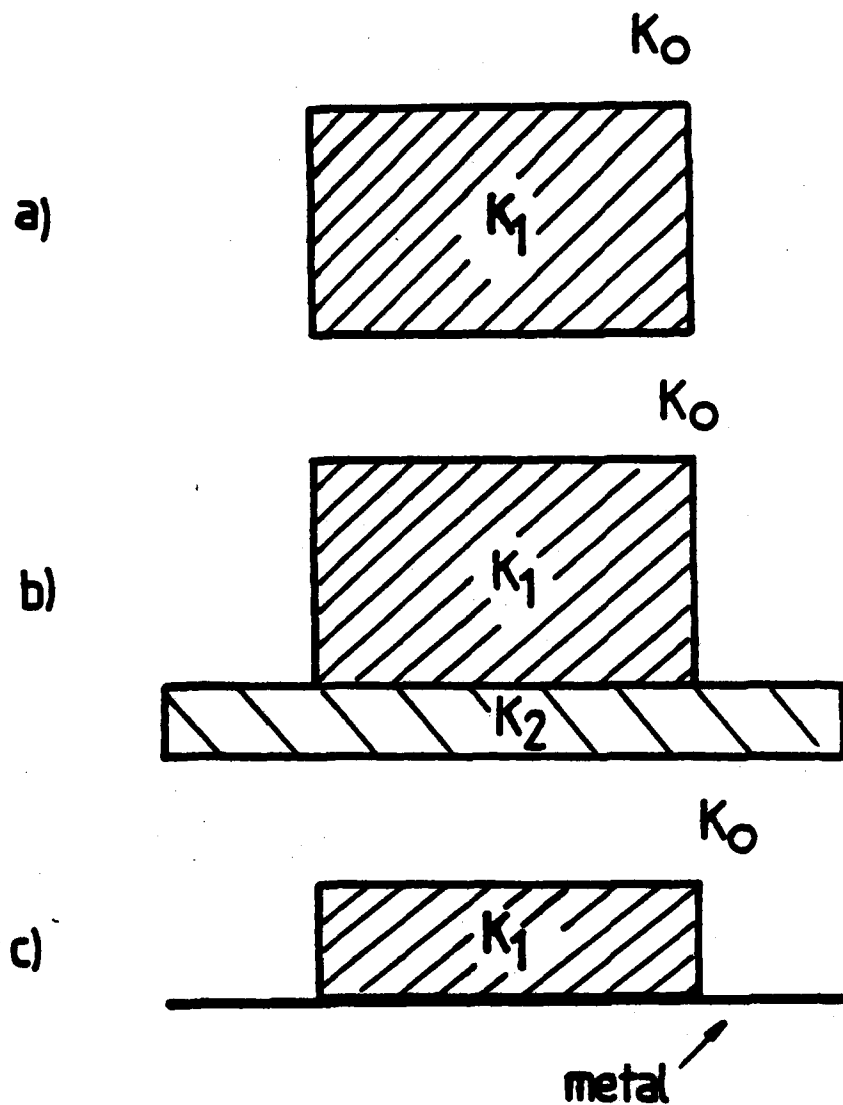


Figure II-1.a. Rectangular dielectric waveguide considered in our numerical analysis; the outer medium is supposed to be of infinite extent.

- b. In practice, the waveguide is often supported by a low-dielectric material which has, to first approximation, little influence on the modes.
- c. The image guide has only some of the modes of the rectangular guide: the metal plane allows only the propagation of the modes that have a vanishing tangential electric field, on the plane surface.

propagation of only those modes of the free-standing guide that have the appropriate symmetry with respect to the metal boundary.

Our objective is to design an efficient numerical tool for computing the propagation characteristics of rectangular dielectric waveguides and obtain accurate representations of the electromagnetic fields.

C. Marcatili's Analysis

Marcatili [Ref. II-3] obtained an approximate analytical solution to the rectangular dielectric waveguide (Fig. II-2) by making the following assumptions:

1. The change of index across the interface is small, i.e.,

$$\sqrt{\frac{\kappa_1}{\kappa_2}} - 1 \ll 1 \quad (\text{II-1})$$

2. The power propagating in the corner areas (cross hatched on Fig. II-2) can be neglected. (This corresponds to assumption that the mode is far from cutoff.)
3. The boundary conditions (continuity of the tangential components of the E- and H-fields) need be satisfied only for the dominant components.

A small index step between the guide and the outer medium will lead to a guided mode that is internally reflected at nearly grazing incidence.

These assumptions result in solutions falling in two families of quasi-plane wave modes, E_{pq}^y and E_{pq}^{x*} . The lower four modes of each family are sketched on Fig. II-3. The field variation is sinusoidal inside the core and exponentially decaying outside of it. The characteristic equations are simple transcendental relations that, far away from cutoff, can be solved in

(*) The superscript denotes the direction of polarization of the electric field and the subscript correspond to the number of maxima respectively in the x- and y-directions.

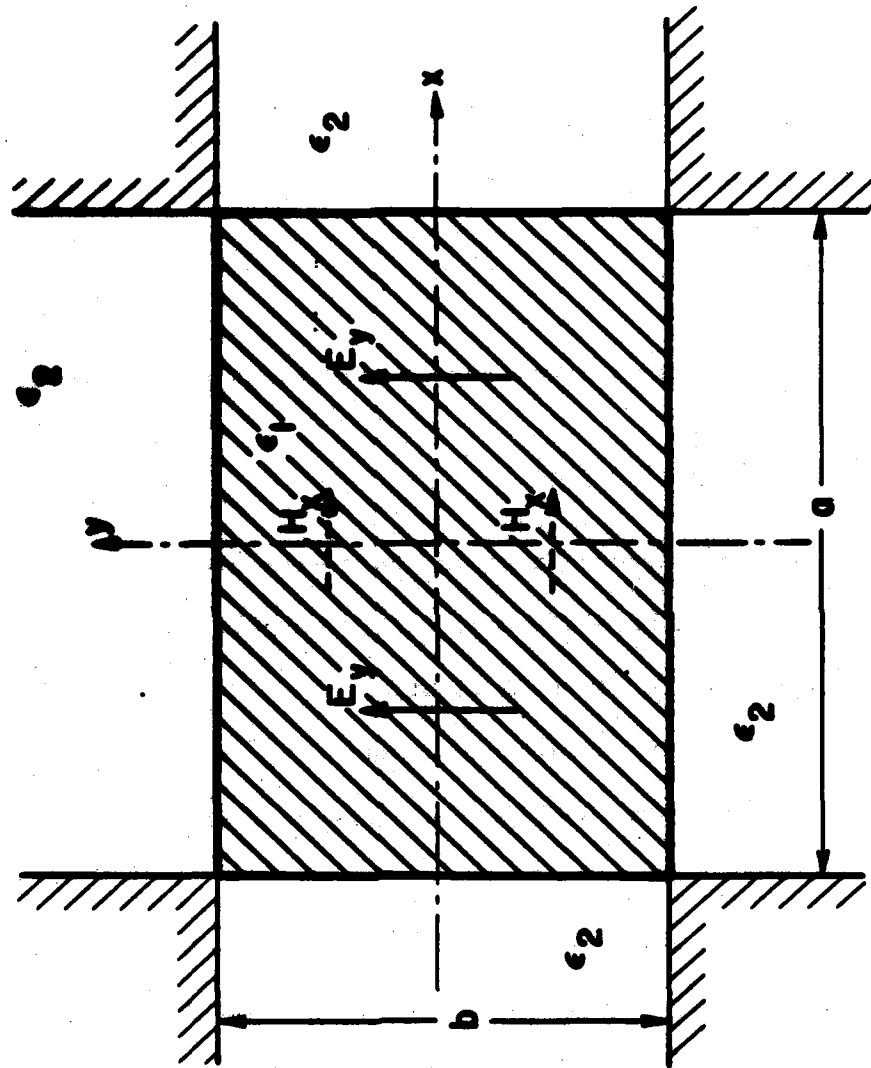


Figure II-2. Marcattili's model for analysis: the corner areas are ignored so that boundary conditions should be satisfied for the dominant field components only on the four sides of the guide.

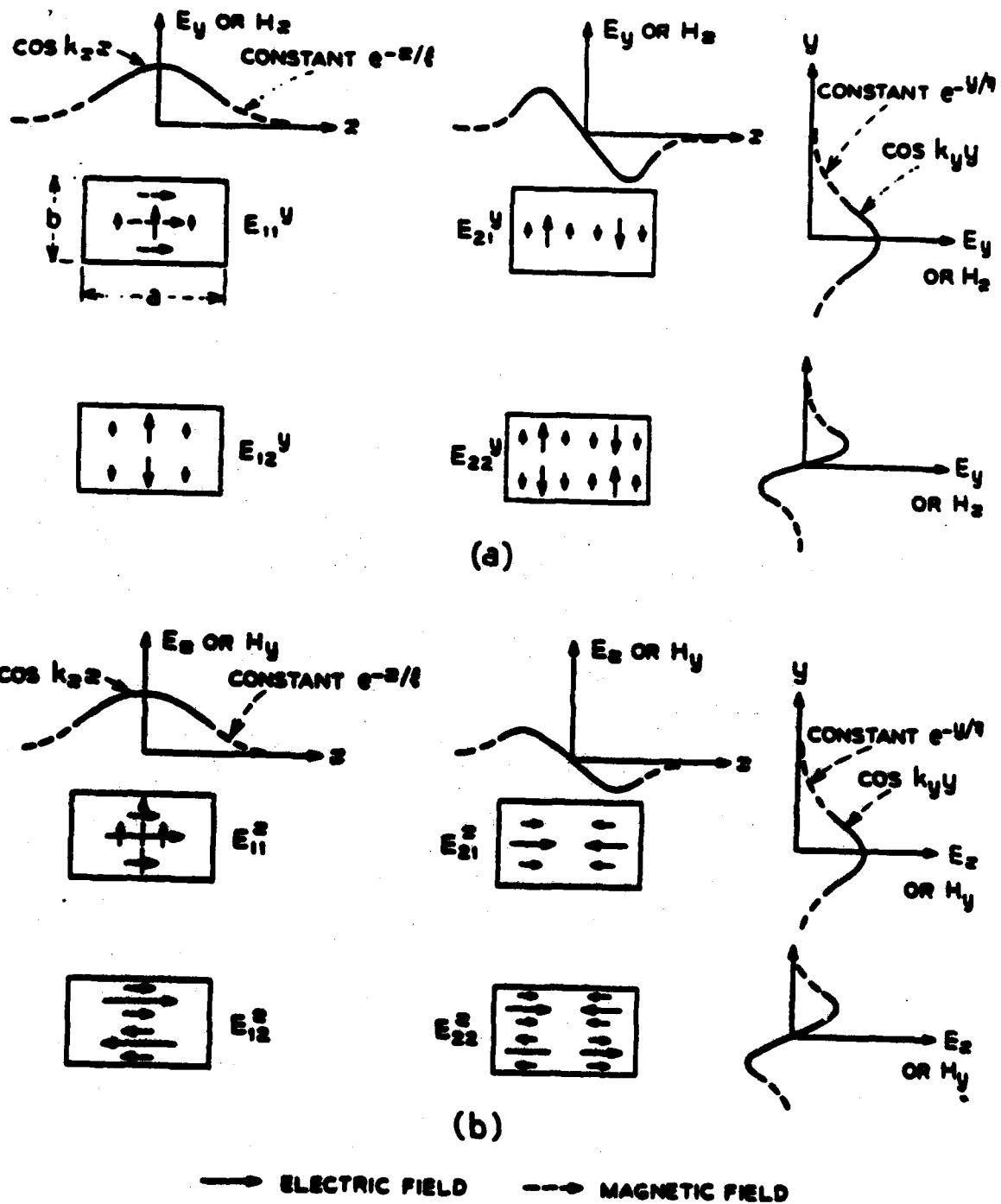


Figure II-3. Dominant quasi-transverse modes: E_{pq}^Y and E_{pq}^X . The superscript refers to the direction of polarisations while the subscripts indicate the number of maxima in each direction.

closed form. They correspond to the characteristic equations of two independent slab problems.

Some authors [Ref. II-6, II-7, II-8], however, apply these solutions to high-permittivity waveguides, for which one or more of Marcatili's assumptions are invalid:

1. The change of permittivity across the interface is large.
2. The power propagating in the corner areas is not negligible.
3. The boundary conditions cannot be satisfied with quasi-plane wave modes.

This is, in essence, similar to the difference between the approximate "linearly-polarized" modes of a weakly-guiding round fiber [Ref. II-10] and the hybrid modes [Ref. II-10] that constitute exact solutions for the round dielectric guide.

D. Other Methods

1. Knox and Toullos [Ref. II-1] have proposed coupling the two independent slab problems that constitute the equivalent of Marcatili's solution. They define an "effective dielectric constant":

$$K_e = K_1 - (k_y/k_0)^2 \quad (II-2)$$

K_1 is the permittivity of region 1 (Fig. II-4), k_y is the separation constant obtained by solving the slab parallel to the x-axis, and k is the free-space wavenumber. To solve the second slab, parallel to the y-axis, the effective dielectric constant, K_e , is used instead of K_1 . This modification is not based upon any theoretical argument and does not resolve the problems encountered with Marcatili's method.

2. Solbach [Ref. II-4] employs a mode-matching technique that proceeds to solve the problem defined in Fig. II-5 as follows:

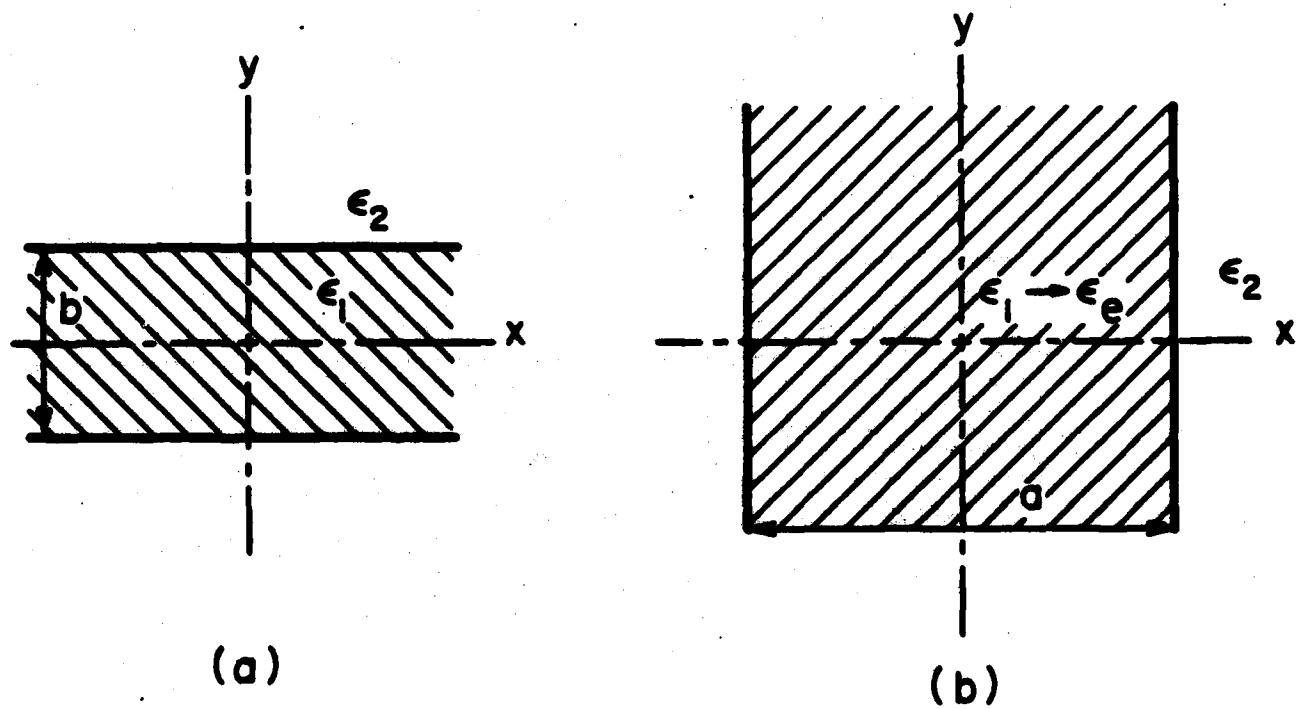


Figure II-4. In the "effective dielectric constant" method, two slab problems, (a) and (b), are coupled.

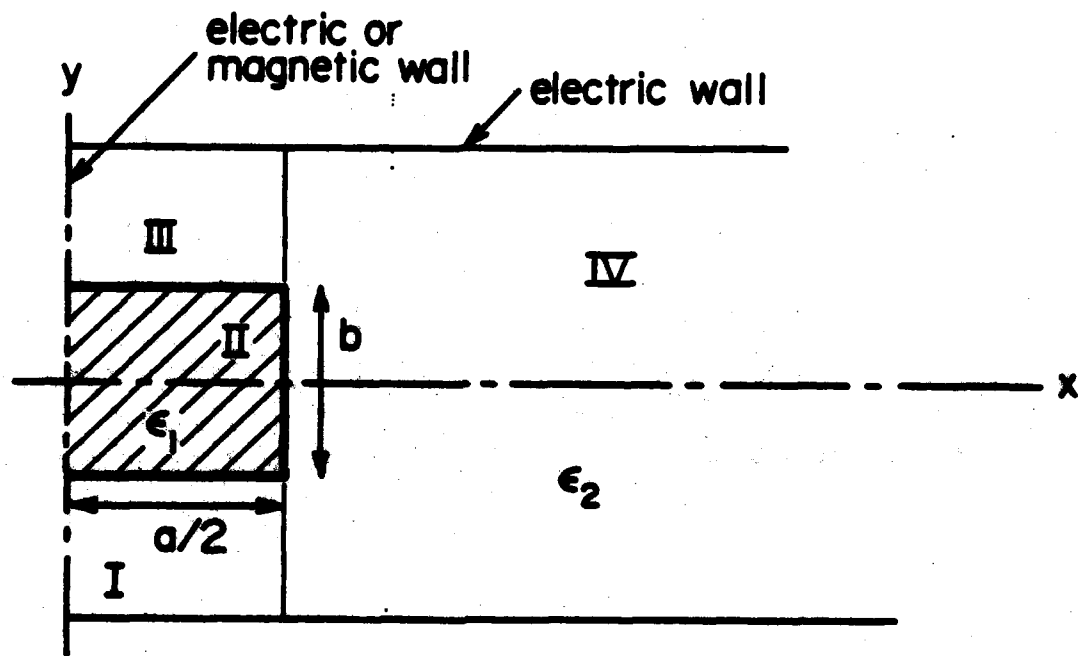


Figure II-5. The mode-matching approach consists in expanding the fields in each subregion in a complete set of waveguide modes and then matching them at the interface.

a. A discrete eigenvalue problem is obtained by placing an electric wall at a finite distance from the dielectric guide.

b. In each region (I-IV), the fields are expanded in a complete set of waveguide modes that satisfy the boundary conditions (electric or magnetic walls) in that region.

c. The coefficients of the expansion (up to a certain order) are obtained by matching the fields at the interfaces.

This method does not appear flexible enough for our purposes and also may present certain convergence problems because of the lack of continuity at the corners.

3. Yeh [Ref. II-5] has proposed a numerical approach based on the finite-elements method that is applicable to a wide range of dielectric waveguide problems. The formulation is very similar to the finite-difference method that we propose, but we believe it is less efficient in the case of relatively simple geometries such as a rectangular waveguide.

B. Finite Differences

Finite-differences (FD) can be applied to a wave propagation problem either by starting from the wave equation or a variationed principle. We investigated both approaches and found that only the latter is numerically stable and accurate.

1. Wave Equation Approach

The usual application of FD is to discretize the differential equations, in this case the wave equations. We define our problem in terms of the longitudinal fields, H_z and E_z . The wave equations for these components are:

$$\nabla_t^2 \phi + k_n^2 \phi = 0$$

for $n = 1, 2$

(II-3)

$$\nabla_t^2 \eta + k_n^2 \eta = 0$$

where

$$\phi = H_z, \quad \eta = \frac{wc_0}{\beta} E_z, \quad H_z \text{ and } E_z \sim \exp(-j\beta z), \text{ and } k_n^2 = K_n k_0^2 - \beta^2 \quad (\text{II-4})$$

At the interface between the two regions, the continuity of the tangential fields must be satisfied. These fields are derived from the longitudinal components. In terms of H_z and E_z , the boundary conditions become:

$$\begin{aligned} -\frac{\partial \phi_2}{\partial x} + \frac{\partial \psi_2}{\partial y} &= \tau \left[-\frac{\partial \phi_1}{\partial x} + \frac{\partial \phi_1}{\partial y} \right] \\ -\frac{\partial \phi_2}{\partial y} + \frac{\partial \psi_2}{\partial x} &= \tau \left[-\frac{\partial \phi_1}{\partial y} - \frac{\partial \psi_1}{\partial x} \right] \end{aligned} \quad (\text{II-5})$$

We then proceed to define a finite problem by enclosing the waveguide in a box with electric walls (perfect conductors) large enough so that it perturbs only minimally the modes of interest. Because of symmetry, we need consider only one quadrant, and we cover that quadrant with a discrete mesh as shown in Figure II-6. At each mesh point, the wave equations are replaced by their finite-difference equivalents.

These equations are valid for all points in region 1 or 2 except at the interfaces. The mesh was chosen so that a row of points lies exactly on each interface. For these points we introduce "image terms" in the finite-difference equations that are then eliminated by using the boundary conditions (continuity of H_z and H_y) expressed in finite-differences. We then obtain a linear eigenvalue problem of the form

$$AX = k_2^2 X \quad (\text{II-7})$$

where X is a vector of the values of H_z and E_z at the mesh points and A is a sparse, real matrix. This problem is solved (on a computer) using standard eigenvalue techniques. However, the matrix A does not have any particular

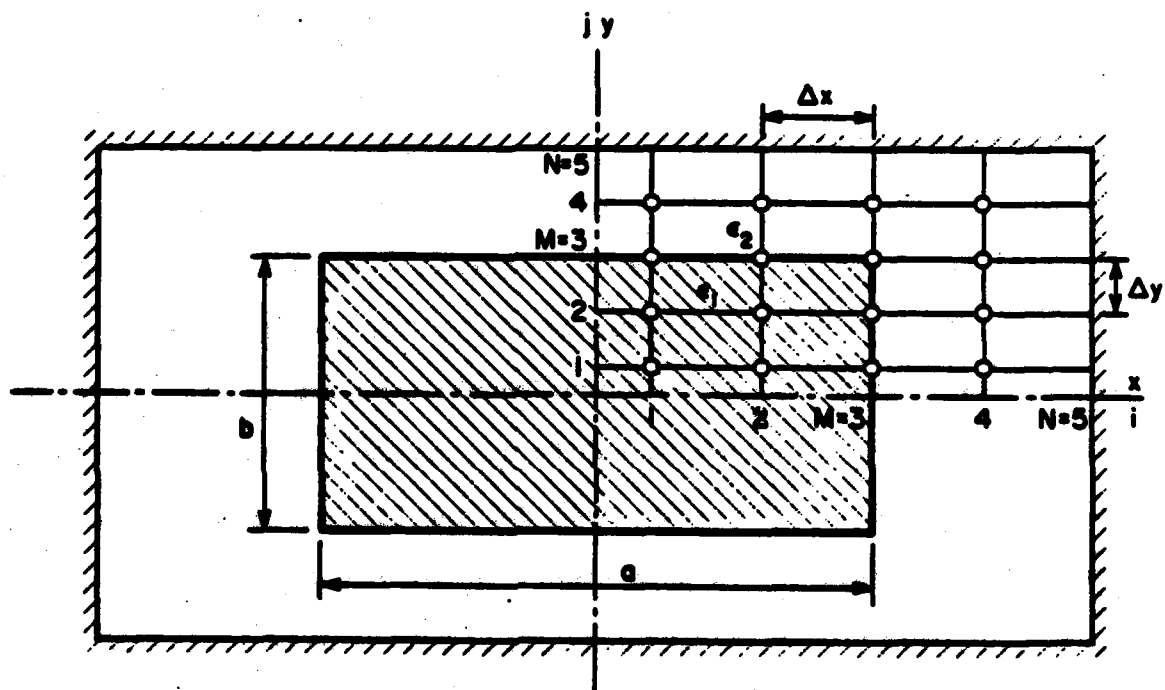


Figure II-6. Grid for the finite-difference calculations. The waveguide is enclosed in a "box". By symmetry, only one quadrant need to be considered. The mesh points lying on the interfaces require a particular treatment.

structural symmetry that would permit a reduction of the numerical labor.

2. Test Case

We tested the method as outlined above by applying it to a one-dimensional problem, the semi-infinite slab. This problem is easily solved analytically [Ref. II-10] and permits us to test the effects of the "box" and our treatment of an interface. Fig. II-7 represents the one-dimensional mesh used and Fig. II-8 shows the good agreement for the field distribution, between the finite-differences solution and the analytical one.

3. Rectangular Guide

When we applied this method to the rectangular guide, we checked the finite-difference solutions by comparing them to either Marcatili's or a round fiber* in the high-frequency limit. In this limit the guide is many wavelengths across and all solutions should converge to the same curve. We then attempted to apply the method to the problem of the rectangular waveguide. We found it to be inaccurate for the limited number of mesh points used ($N = 9$ in each linear dimension). Since the size of matrix A increases as N^2 , computer storage limitations prevented an increase in N .

4. Variational Approach

An other approach is to start from a variational quantity and discretize it by applying finite-differences. It is well known [Refs. II-5, II-11] that for propagating electromagnetic modes, the following variational principle holds:

$$\delta \tau = 0$$

where

(*) The round fiber is chosen so that its cross-section has the same area as the corresponding square guide that is considered.

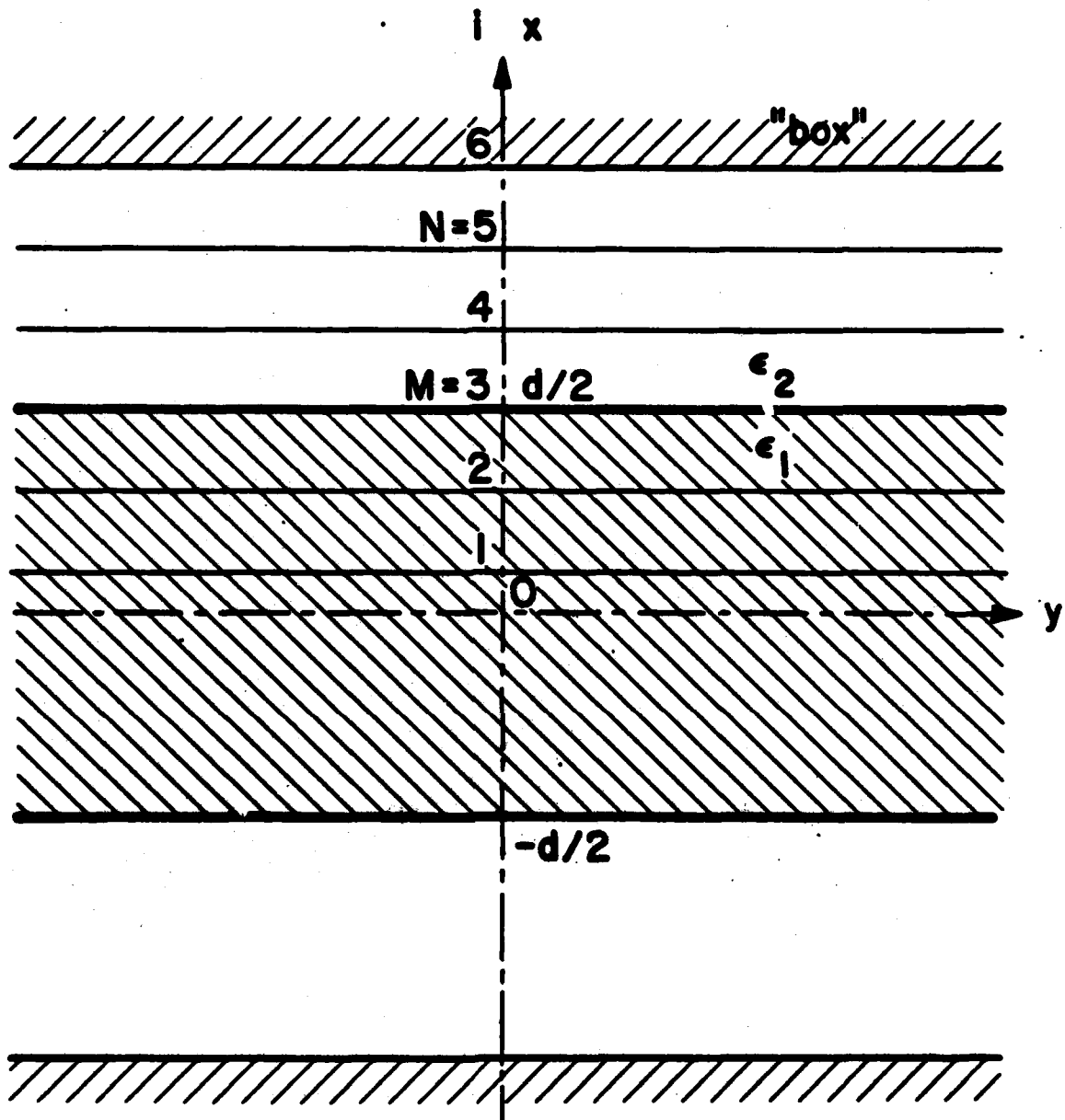


Figure II-7. One-dimensional mesh for the test of the FD method with a slab problem.

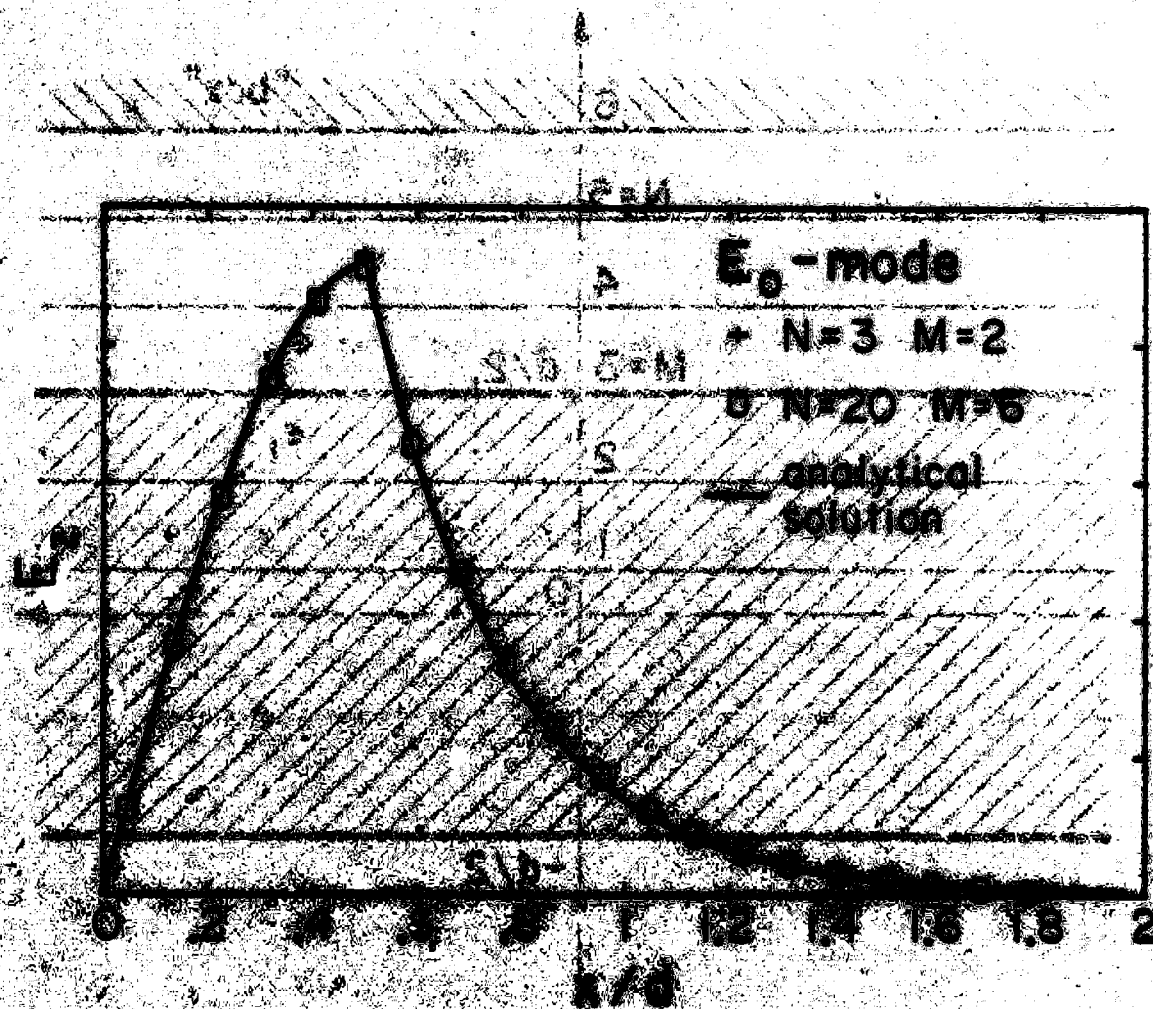


Figure 11-4. The longitudinal electric field, of the dominant E₀-mode, plotted versus normalized distance calculated using the data of Fig. 11-7. The comparison between the exact analytical solution and the 10-mesh calculation is shown.

$$J = \iint_S \left\{ \left[\frac{\beta c}{\omega} \right]^2 \tau K_1 \nabla_t \psi_1^2 + \tau_1 \nabla_t \phi_1^2 + 2 \left[\frac{\beta c}{\omega} \right]^2 \tau \left[\frac{\partial \psi}{\partial x} \frac{\partial \phi}{\partial y} - \frac{\partial \phi}{\partial x} \frac{\partial \psi}{\partial y} \right] - k_0^2 \left[\phi^2 + \left[\frac{\beta c}{\omega} \right]^2 K \psi^2 \right] \right\} ds \quad (\text{II-7})$$

with $\phi = H_z$ and $\psi = (\omega c_0 / \beta) E_z$.

If we consider a rectangular element, S_1 , as depicted on Fig. II-9, such that the permittivity is constant inside the element, we can compute the contribution of S_p to J by using finite-differences:

$$\begin{aligned} \iint_{S_p} \phi^2 ds &= \frac{1}{4} h_1 h_2 \left[\phi_1^2 + \phi_2^2 + \phi_3^2 + \phi_4^2 \right] \\ \iint_{S_p} |\nabla_t \phi|^2 ds &= \frac{1}{2} h_1 h_2 \left\{ \left[\left[\frac{\phi_4 - \phi_2}{h_1} \right]^2 + \left[\frac{\phi_3 - \phi_1}{h_1} \right]^2 + \left[\frac{\phi_4 - \phi_3}{h_2} \right]^2 + \left[\frac{\phi_2 - \phi_1}{h_2} \right]^2 \right] \right\} \\ \iint_{S_p} \frac{\partial \phi}{\partial y} \frac{\partial \psi}{\partial x} ds &= \frac{1}{4} h_1 h_2 \left[\frac{\phi_4 - \phi_3}{h_2} + \frac{\phi_2 - \phi_1}{h_2} \right] \left[\frac{\psi_4 - \psi_2}{h_1} + \frac{\psi_3 - \psi_1}{h_1} \right] \end{aligned} \quad (\text{II-8})$$

For the problem of the rectangular guide we can then define a mesh that covers the area of interest with rectangular elements (Fig. II-10). J is obtained by adding the contribution of each element. We note that no special treatment is required for the interfaces, as J contains the continuity conditions. By setting to zero the partial derivatives of J with respect to the field values H_z and E_z at each mesh points, we obtain a linear eigenvalue problem of the form

$$AX = k_2^2 BX \quad (\text{II-9})$$

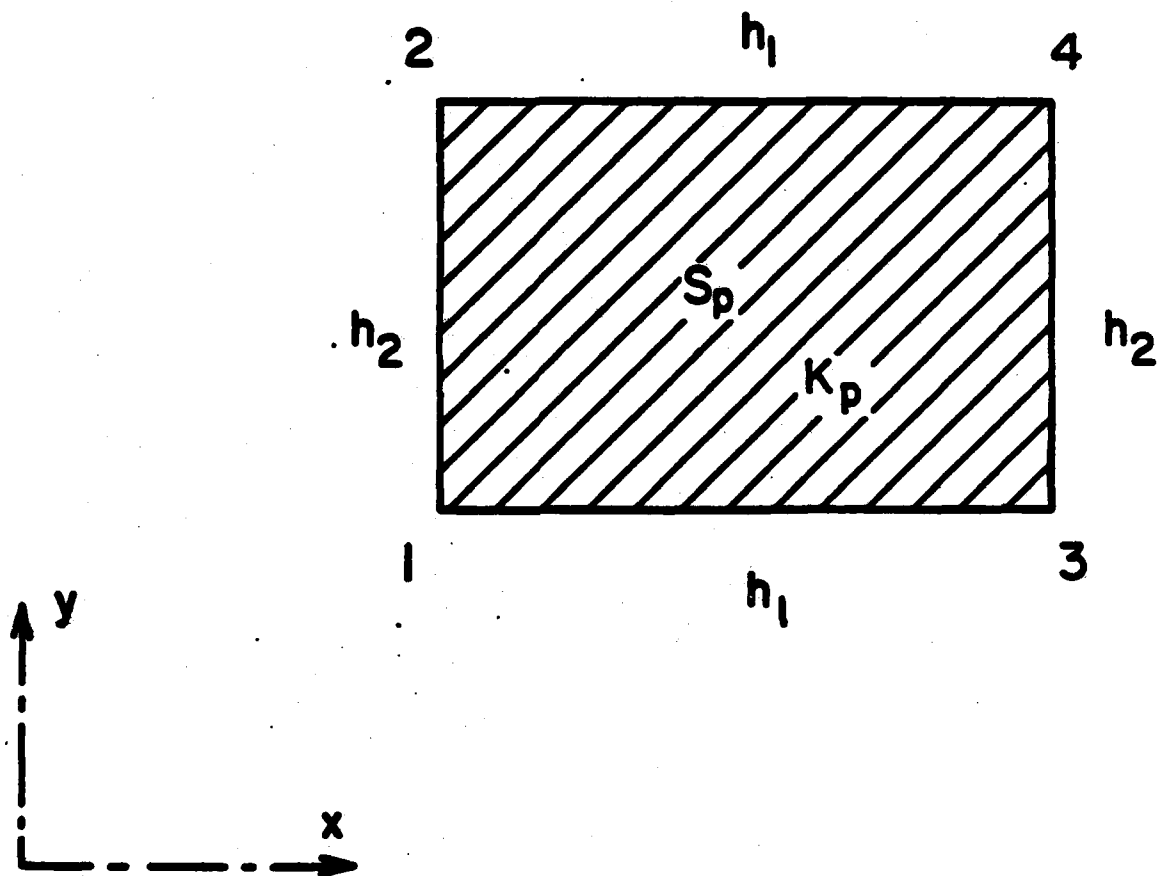


Figure II-9. Typical rectangular element for the finite difference computation.

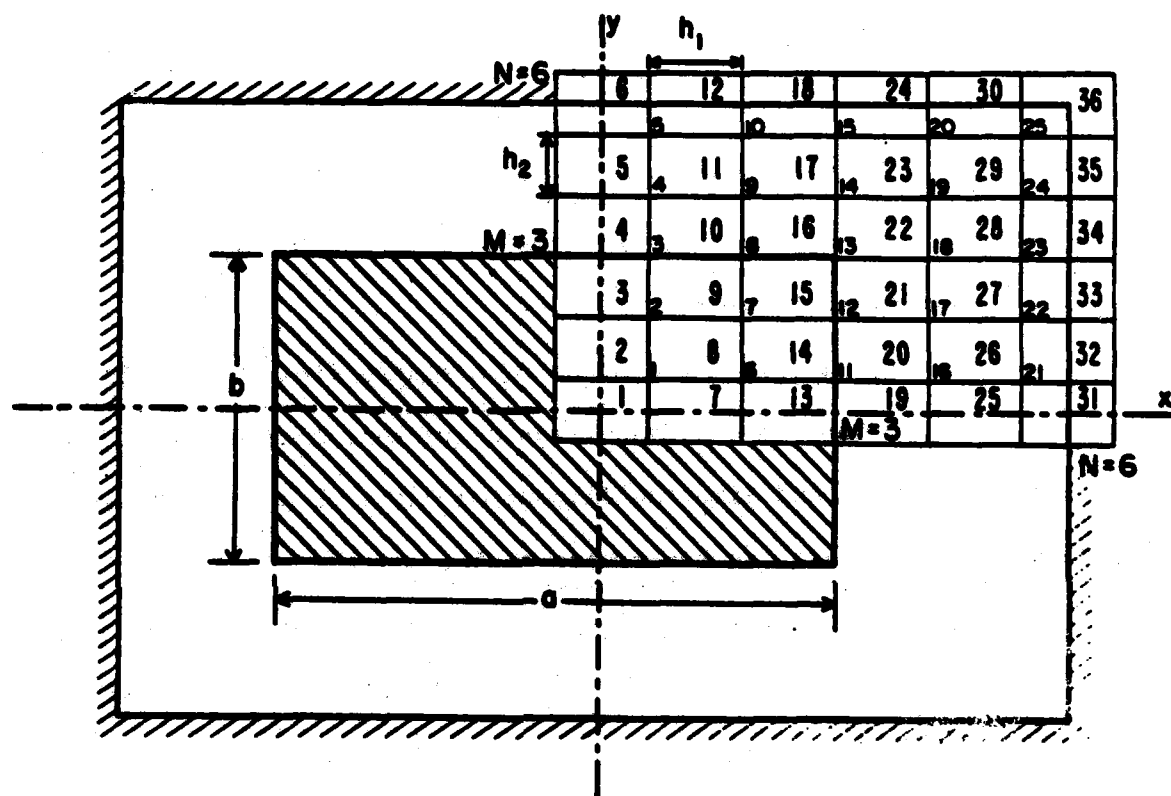


Figure II-10. Grid for finite-difference calculations based on the variational approach. One quadrant is "covered" by rectangular elements. The contribution of each element is added up to form the matrix A . No special treatment is required at the interfaces.

where X is a vector of ordered field values, A is a symmetric band matrix and B is a positive definite diagonal matrix. By a simple similarity transformation,

$$B^{-1/2} A B^{-1/2} = A' \quad (\text{II-10})$$

we reduce the problem to

$$A'X = k_2^2 X \quad (\text{II-11})$$

where A' is now a symmetric band matrix. This structure allows us to store the matrix A more efficiently and thus permits us to use a very fine mesh.

5. Numerical Results

We have analyzed the modes of a square dielectric guide because it allows us to compare the dispersion characteristics with the theory proposed by Marcatili and with the dispersion curve of a round fiber chosen to have the same diameter as the square guide.

Figure II-11 presents the dispersion curve, as computed by these three methods, for the dominant mode of a dielectric guide made of Teflon ($K_1 = 2.1$). At high frequency, as we expected, the dispersion curves are not distinguishable. They deviate at lower frequencies because Marcatili's theory predicts a sharp cutoff, while the dominant mode of a round fiber has no cutoff frequency. The finite difference calculation gives an intermediate result. We are limited, at low frequency, by the size of the mesh that we can treat; the outer box must be further removed in order to limit its influence on the mode. The same calculations for a high-dielectric constant guide (made of GaAs, $K_1 = 13.1$), show that Marcatili's theory and the round fiber approximation give nearly the same curve that differs noticeably from the FD results (Fig. II-12), only in the intermediate frequency range, between the "close to cutoff" and "far from cutoff" regions.

DOMINANT MODE OF A SQUARE GUIDE

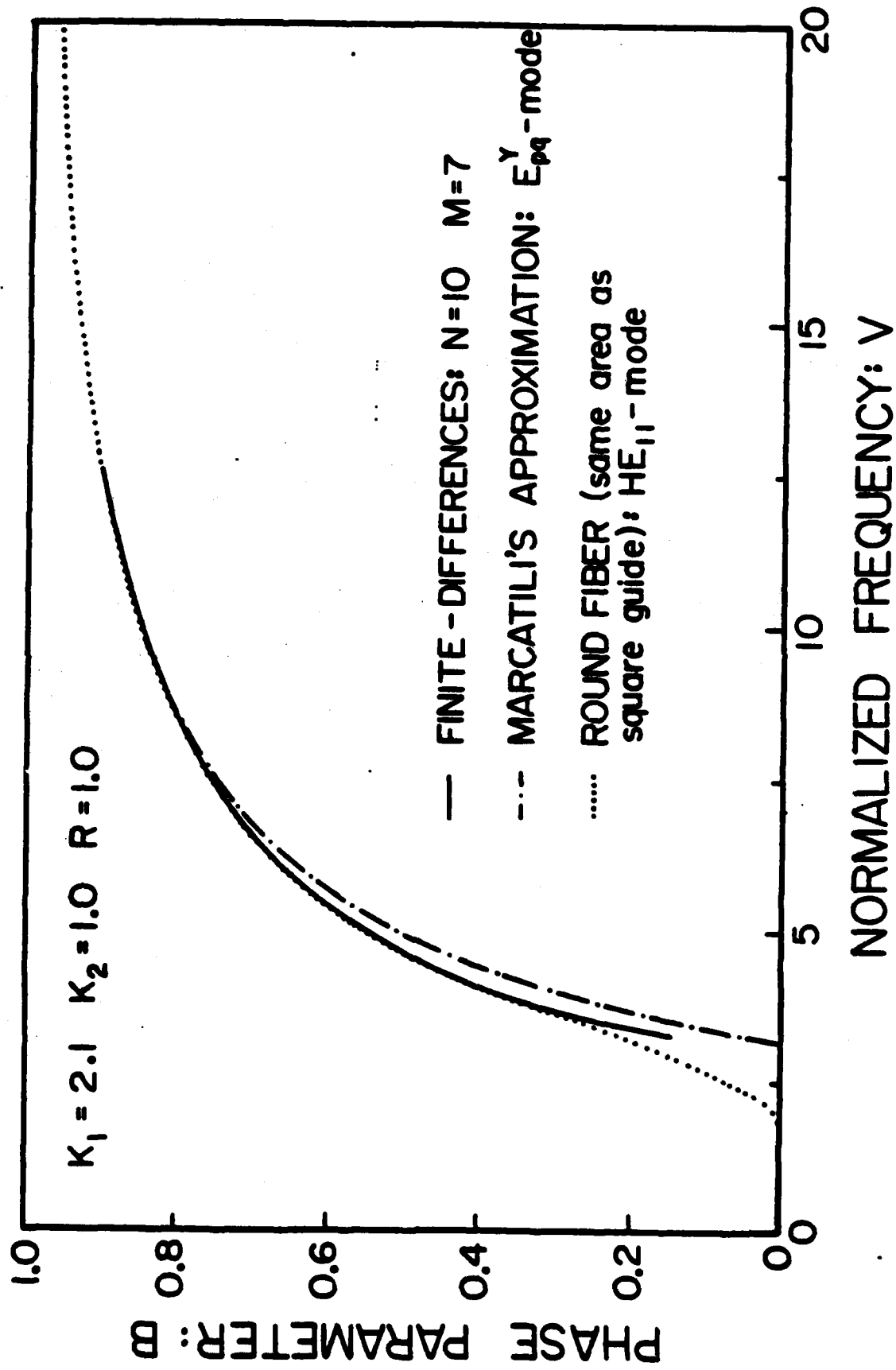


Figure II-11. Dispersion curve of the dominant mode of a square dielectric waveguide, as computed by three methods: (1) FD (100 elements); (2) Marcatili's theory: $p=1, q=1$; (3) round guide: HE_{11} -mode.

DOMINANT MODE OF A SQUARE GUIDE

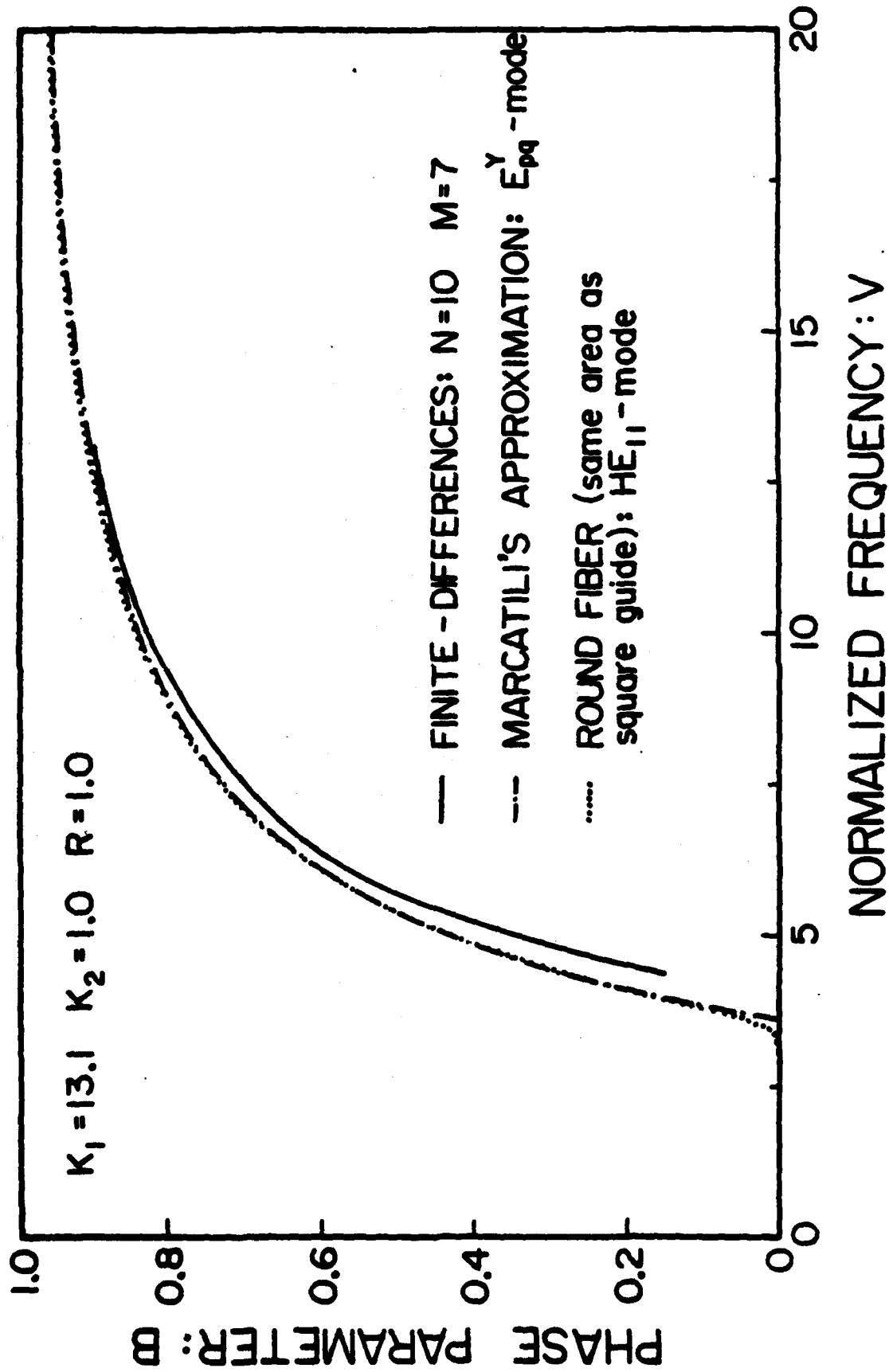


Figure II-12. Dispersion curve of the dominant mode of a square dielectric waveguide. The same methods were used as depicted on Fig. II-11 (GaAs $K_1 = 13.1$). The waveguide is of relatively high dielectric constant.

F. Future Work

We are working on a package of numerical routines that will allow us to extract the dominant eigenvalues and corresponding eigenvectors from a symmetric band matrix that is stored in a compact array. This will permit us a large increase in the grid size. We will make a detailed analysis of the fields of a rectangular dielectric waveguide and compare them to Marcattili's solutions.

REFERENCES FOR SECTION II

- II-1. R. M. Knox and P. P. Toullos, "Integrated Circuits for the Millimeter Through Optical Frequency Range," Proc. of the Symp. Submillimeter Waves, New York, March 1970.
- II-2. Shuichi Shindo and Takao Itanami, "Low-Loss Rectangular Dielectric Image Line for Millimeter-Wave Integrated Circuits," IEEE Trans. Microwave Th. Tech., vol. MTT-26, Oct. 1978, pp. 747-751.
- II-3. E. A. J. Marcotili, "Dielectric Rectangular Waveguide and Directional Coupler for Integrated Optics," Bell Syst. Tech. J., Sept. 1969, pp. 2071-2102.
- II-4. Klaus Solbach, "The Electromagnetic Fields and the Phase Constants of Dielectric Image Lines," IEEE Trans. Microwave Th. Tech., vol. MTT-26, Apr. 1978, pp. 266-274.
- II-5. C. Yeh, K. Ha, S. B. Dong and W. P. Brown, "Single-Mode Optical Waveguides," Appl. Opt., vol. 18, May 1979, pp. 1490-1504.
- II-6. Harold Jacobs and Metro M. Chrepta, "Electronics Phase Shifter Millimeter-Wave Semiconductor Dielectric Integrated Circuits," IEEE Trans. Microwave Th. Tech., vol. MTT-22, Apr. 1974, pp. 411-417.
- II-7. Kenneth L. Klohn, Robert E. Horn, Harold Jacobs and Elmer Freibergs, "Silicon Waveguide Frequency Scanning Linear Array Antenna," IEEE Trans. Microwave Th. Tech., vol. MTT-26, Oct. 1978, pp. 764-773.
- II-8. Chi H. Lee, S. Mak and A. P. DeFonzo, "Optical Control of Millimeter-Wave Propagation in Dielectric Waveguides," IEEE J. Quant. Electr., vol. QE-16, March 1980, pp. 277-288.
- II-9. J. S. Hornsby and A. Gopinath, "Numerical Analysis of a Dielectric-Loaded Waveguide with a Microscopic Line--Finite-Difference Methods," IEEE Trans. Microwave Th. Tech., vol. MTT-17, Sept. 1969, pp. 684-690.

- II-10. H. G. Unger, "Planar Optical Waveguides and Fibres," Clarendon Press, Oxford, 1977.
- II-11. Douglas G. Corr and J. Brian Davies, "Computer Analysis of the Fundamental and Higher Order Modes in Single and Coupled Microstrip," IEEE Trans. Microwave Th. and Tech., vol. MTT-20, Oct. 1972, pp. 669-678.

III. ELECTRO-OPTIC DEVICES IN DIELECTRIC WAVEGUIDE (M. B. Klein*)

A. Introduction

In recent years, integrated circuit techniques have become increasingly important in implementing components and subsystems at millimeter wavelengths. A number of passive and active devices have been demonstrated in dielectric waveguide including directional couplers, filters, phase shifters, scanning antennas, detectors and sources. In most cases, the active devices studied required careful mounting of a discrete electrical device in close proximity to the waveguide structure in a way which optimizes coupling to the waveguide. In this discussion we describe active devices in dielectric waveguide which can be realized by direct electrical control of the bulk dielectric properties of the transmission medium. These devices have intrinsic high speed, and are directly compatible with common dielectric waveguide structures.

Two general classes of materials have bulk dielectric properties which can be electrically controlled: semiconductors and electro-optic crystals. In semiconductors, the generation of carriers leads to changes in both the real and imaginary parts of the complex permittivity. These effects have been used to construct phase shifters [Refs. III-1, III-2, III-3] and switches [III-4] in dielectric waveguide using materials such as gallium arsenide and silicon. Large modulation amplitudes have been observed, but the switching speed in most cases is limited by the carrier recombination time to values in the range 0.1-1 μ sec. In electro-optic materials (or nonlinear dielectrics) an applied voltage produces a direct change in the real (and imaginary) part of the dielectric constant, due to distortions of the crystal lattice. Materials of interest in this category include

(*) Member of the Technical Staff, Hughes Research Laboratories, Malibu, CA.

ferroelectric crystals which are commonly used for modulation in the visible such as LiNbO_3 and LiTaO_3 . In these materials the medium response time is instantaneous at frequencies up to 300 GHz, and the modulation speed is limited only by circuit conditions. Because of their intrinsic high speed response, nonlinear materials are also promising for frequency mixing applications at frequencies throughout the millimeter band.

The usefulness of nonlinear materials for frequency mixing in the millimeter band was first demonstrated by Boyd, et al. [Refs. III-5, III-6] in experiments conducted at 56 GHz. Around the same time electro-optic modulation was demonstrated in LiNbO_3 at 126 GHz [Ref. III-7] and in LiTaO_3 at 890 GHz [Ref. III-8].

More recently we have measured the electro-optic coefficients for several orientations in LiNbO_3 and LiTaO_3 at 94 GHz [Ref. III-9]. In each of the above experiments the sample was either mounted in free space or in conventional metal waveguide. Free space mounting requires large samples to minimize diffraction loss, while mounting in conventional waveguide introduces severe dimensional tolerances and requires a feedthrough for modulating voltages. If instead the electro-optic material is prepared in the form of dielectric waveguide, then the requirement for large samples or critical dimensional tolerances is removed, and compatibility with other integrated circuit components is facilitated.

The discussion in this section presents the results of our analysis and experiments on electro-optic devices in dielectric waveguide. In Part B we describe the electro-optic properties of ferroelectric materials, and in Part C candidate waveguide structures for phase shifting are considered. Part D describes experiments on a LiNbO_3 E-guide phase shifter at 94 GHz, and in Part E our analysis of other control devices is presented. Part F discusses the prospects for improved materials, and our conclusions and future plans are discussed in Part G.

B. Electro-Optic Properties of Ferroelectric Materials

Phase shifters using the electro-optic effect in bulk crystals are commonly used in the visible, and have speeds limited only by circuit conditions. In this work we describe our studies of electro-optic phase shifting at 94 GHz. We have used a phenomenological model to calculate electro-optic coefficients for a number of materials, and have measured electro-optic coefficients for a number of orientations in LiNbO_3 and LiTaO_3 .

The phase shift for a transverse modulator is given by

$$\Gamma = \frac{\pi L}{\lambda} \frac{V}{D} n^3 r \quad (\text{III-1})$$

where L is the crystal length, V is the applied voltage, D is the electrode spacing, n is the microwave refractive index and r is the electro-optic coefficient. The specific dependence of both n and r on the orientation of the microwave and low frequency electric fields is ignored here (for brevity) but is properly accounted for in our later calculations. In order to characterize a given electro-optic material for phase shifting applications, we will make use of a figure of merit R , defined by

$$R = n^3 r \quad (\text{III-2})$$

One important reason for utilizing the electro-optic effect is that the electro-optic coefficients for certain materials in the microwave region are much larger than those in the visible [Ref. III-6]. This enhancement is an important requirement, since the expected phase shift varies inversely with wavelength and would otherwise be small in the far infrared and near millimeter region. It has been shown that crystals with the largest microwave electro-optic (and nonlinear) coefficients are those with the largest values of linear susceptibility [Refs. III-5, III-6]. In the microwave region the linear susceptibility can be much larger than in the visible, due to the contribution from lattice vibrations. More specifically, the electro-optic

coefficient for a given crystal in the microwave region can be written as

$$r = 4\chi_1\delta \quad (III-3)$$

where χ_1 is the ionic (or lattice) contribution to the linear susceptibility, and δ is an empirical factor which is nearly constant for a wide range of materials and orientations. In low loss materials, the requirement for large values of χ_1 is equivalent to requiring large values of ϵ_r , the low frequency relative dielectric constant. The importance of high ϵ_r materials is emphasized when we note (using $r \propto \epsilon_r^{-1/2}$) that the figure of merit $R \sim \epsilon_r^{5/2}$. In ferroelectrics, values of ϵ_r in the range 20-100 are quite common.

Two materials of particular interest for device applications are LiNbO_3 and LiTaO_3 . Large samples of these materials are available, and the microwave losses are low. Measured linear parameters and values of the figure of merit R for several orientations in LiNbO_3 and LiTaO_3 [Ref. III-9] are given in Table III-1.

C. Waveguide Structures for Phase Shifting

We now wish to consider possible dielectric waveguide structures for the particular case of electro-optic phase shifting. A candidate structure should be judged against 3 major requirements:

- (a) The structure must comprise two (or more) metallic conductors for application of modulating voltages;
- (b) The microwave and modulating fields must be confined in the dielectric for optimum interaction;
- (c) The electric field lines should be straight and parallel to a single principal crystal direction to avoid phase interference effects.

In Table III-2 we have listed four common structures and the particular requirements satisfied by each. It is clear that H-guide is the preferred

Table III-1. Measured Values of the Linear Parameters and Figure of Merit for LiNbO_3 and LiTaO_3 .

11473-8R1





STRUCTURE	CONFIGURATION	REQUIREMENTS SATISFIED
IMAGE GUIDE		B, C
SLOT LINE		A, (B)
MICROSTRIP		A, B
H-GUIDE (TE MODES)		A, (B), C

Table III-2. Four Millimeter Dielectric Waveguide Structures.

11473-7

MATERIAL	POLARIZATION	MICROWAVE REFRACTIVE INDEX	POWER ABSORPTION COEFFICIENT (cm^{-1})
LiNbO_3	ORDINARY	6.7	~ 0.2
	EXTRAORDINARY	5.2	~ 0.2
LiTaO_3	ORDINARY	6.5	~ 0.4
	EXTRAORDINARY	6.5	~ 0.9

(a)

MATERIAL	ORIENTATION	FIGURE OF MERIT n^3_r (10^{-7} cm/VOLT)
LiNbO_3	333	5.0
	113	4.8
	222	5.7
LiTaO_3	333	15.0
	113	5.2

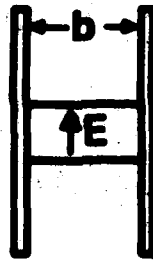
(b)

choice (parallel-plate transmission line partially loaded with dielectric). It is important to distinguish between the hybrid modes and the modes in H-guide (see Fig. III-1). The hybrid modes [Ref. III-10] have components of electric field in the longitudinal direction and in both transverse directions, although the dominant transverse component is parallel to the metallic conducting plates. The multiple components of electric field are a disadvantage in that interferences in the electro-optic phase shift can be produced (violation of requirement C above). One advantage of the hybrid modes is that the electric field is small at the metallic walls, and thus wall losses are low. However, at the present stage of development, material losses are dominant and the low wall losses of the hybrid modes cannot be exploited. The TE modes [Ref. III-10, III-11] have a single component of electric field directed normal to the metallic planes. Wall losses are larger than for the hybrid modes, but still less than material losses. One important advantage of the TE modes is that the lowest order mode (designated TE_{10}) has no cutoff, so that energy can be coupled in or out of the dielectric medium. This is especially useful for radiative devices such as scanning antennas.

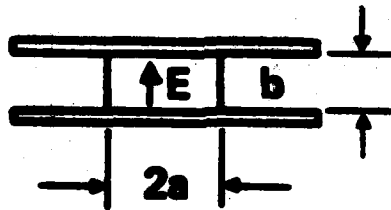
We have calculated the mode cutoff properties [Ref. III-11] of an H-guide filled with $LiNbO_3$ (Y-axis normal to metallic plates, and the results are plotted in Fig. III-2. The lowest order hybrid mode is cutoff for $b/\lambda_0 \leq 0.1$, while the TE modes propagate for all values of b . We also show the cutoff width for the TE_{30} mode, which is the first higher order TE mode which is likely to be excited in our experiments. The sample dimensions we have chosen (see below) could allow the lowest order hybrid mode to propagate, but the input radiation is orthogonally polarized to the dominant polarization of the hybrid mode, so the coupling coefficient to this mode should be very small.

We have fabricated $LiNbO_3$ samples with two different cross sections:

11473-9



(a)



(b)

Figure III-1. Electric field orientation for (a) hybrid mode and (b) TE mode in the H-guide structure.

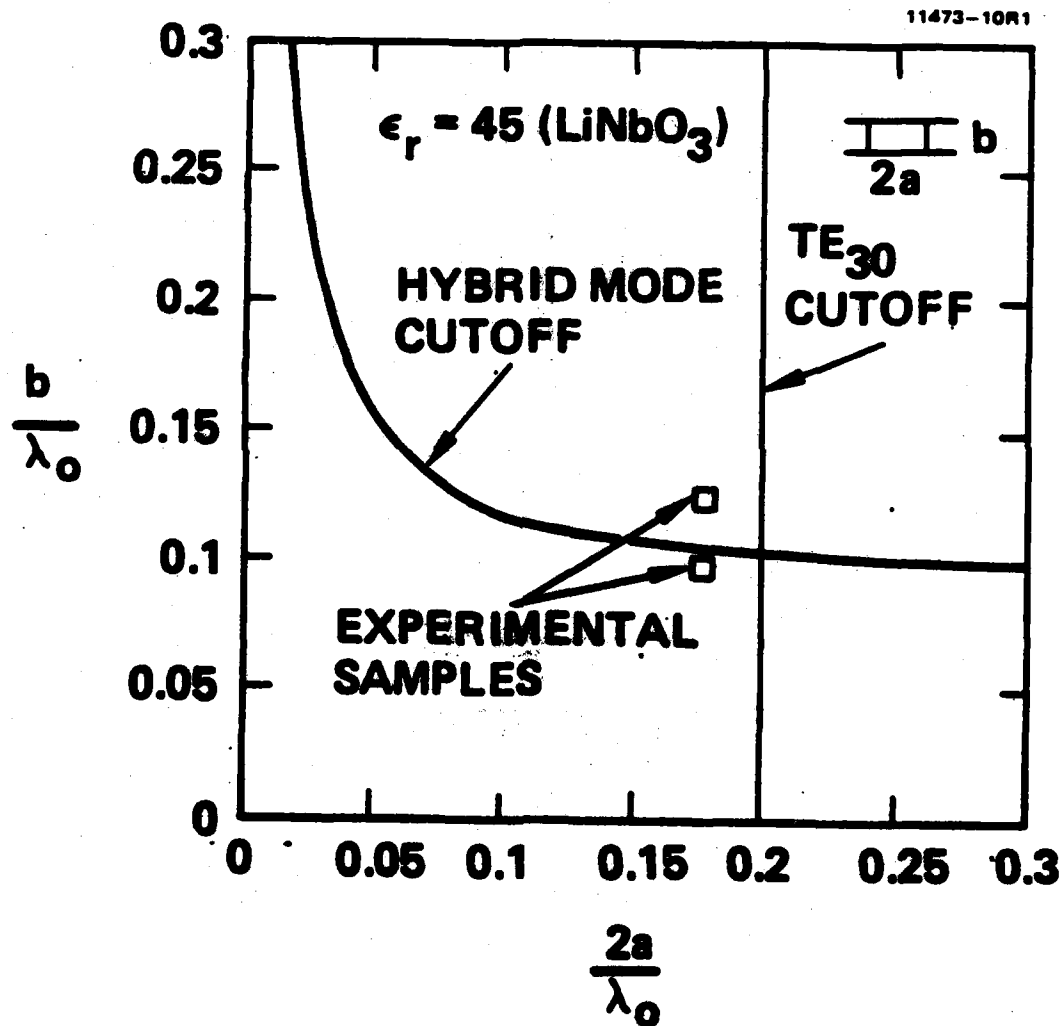


Figure III-2. Mode cutoff properties in LiNbO_3 H-guide.

Sample 1: $2a = 0.55$ mm, $b = 0.30$ mm,

Sample 2: $2a = 0.55$ mm, $b = 0.40$ mm.

A number of TE_{10} mode properties were calculated for the two sample cross sections:

- (1) lateral decay distance of fields into free space = 0.06 mm normalized guide wavelength

$$\frac{\lambda_g}{(\lambda_0/\sqrt{\epsilon_r})} = 1.09 \quad ,$$

- (2) Impedance: Sample 1: 60 OHMS

Sample 2: 80 OHMS

- (3) Power absorption coefficient normalized to that of plane wave in $LiNbO_3$:

$$\frac{\alpha}{\alpha_{plane}} = 0.97 \quad (\alpha_{plane} = 0.2 \text{ cm}^{-1}) \quad ,$$

- (4) Induced phase shift normalized to that of plane wave in $LiNbO_3$:

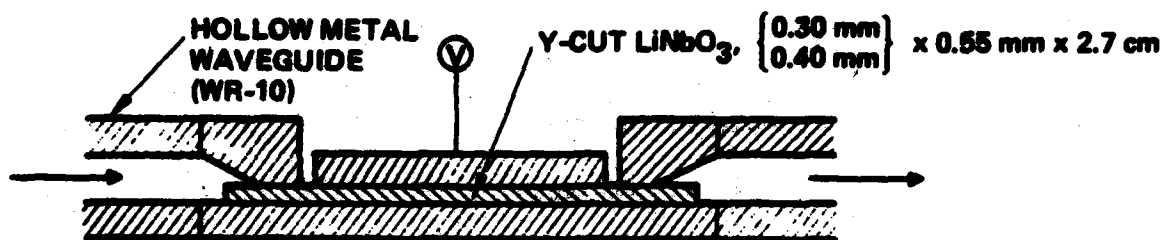
$$\frac{\Gamma}{\Gamma_{plane}} = 0.98 \quad (\Gamma_{plane} = 12.5^\circ/\text{cm for } 20 \text{ kv/cm field}).$$

The above properties indicate that the radiation in the TE_{10} mode is well confined within the $LiNbO_3$, and has nearly identical properties to those of an unbounded plane wave in the material.

D. $LiNbO_3$ H-Guide Phase Shifters at 94 GHz

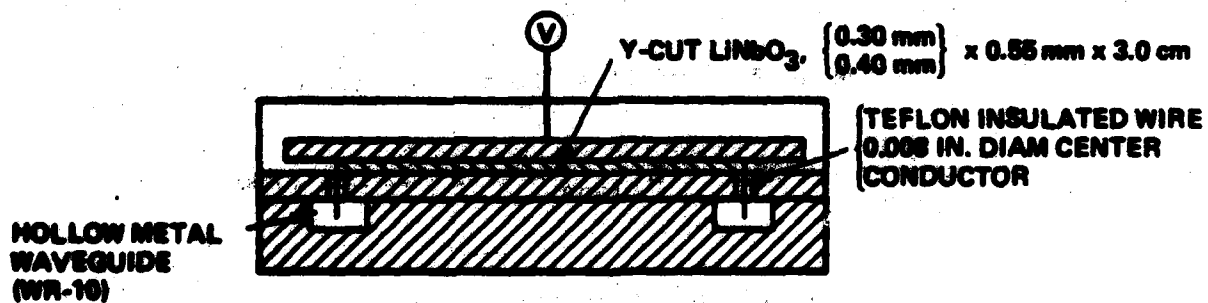
We have designed and constructed two $LiNbO_3$ H-guide phase shifters, differing only in their means of coupling from WR-10 hollow metal waveguide to $LiNbO_3$ H-guide. The first device utilizes end coupling, and is shown in Figure III-3a. The $LiNbO_3$ sample is mounted on a flat metal ground plane, which is also the bottom portion of the hollow metal waveguide. The sample

11473-13



(a)

11473-14



(b)

Figure III-3. Configurations of two different LiNbO_3 phase shifters employing
 (a) direct wave coupling to WR-10 waveguide and
 (b) coupling through probes.

extends into the metal waveguide; the latter tapers down to the same height as the LiNbO_3 , and to twice the width. The upper plate of the H-guide is isolated from the surrounding metal structure and is held in place by spring loading. This device is simple to construct and align, and has a wide bandwidth, due to the lack of tuning elements. One disadvantage is that the discontinuity in the upper plate increases the VSWR and reduces the coupling efficiency.

The modulation performance and insertion loss of the above device were measured by insertion of the device into the active arm of a waveguide phase bridge. The bridge was first balanced by adjusting the variable attenuator in the reference arm for maximum fringe contrast. An adjustable phase shifter in the reference arm was then set at the midpoint of the fringe pattern, i.e., the linear region. For this bias condition an ac voltage applied to the crystal causes an amplitude modulation on the detector output at the applied frequency (1 kHz). The fractional modulation can then be related directly to the peak induced phase shift.

Our device measurements were made using the smaller cross-section sample. This insertion loss was 12 dB, of which only 3 dB is due to sample absorption. This suggests that further improvement in transition and coupling design could lead to a considerable reduction in insertion loss. For a peak applied voltage of 1000 V, the amplitude modulation was 67%, and the induced phase shift was 56° peak-to-peak, in good agreement with theory, based on the electro-optic coefficients given in [Ref. III-9].

The second phase shifter which we designed and tested follows the design of a device described and demonstrated at 200 MHz by Cohn and Eikenberg [Ref. III-12]. The key element of this device is that probe coupling is used instead of end coupling to WR-10 waveguides. A cross section of our device is shown in Fig. III-3b. A short section of teflon insulated wire with insulation

removed at each end provides the connection between the hollow metal waveguide and the LiNbO_3 H-guide. One end of the wire probes the field in the hollow metal waveguide. The center (insulated) section is a coaxial waveguide connection, and the opposite end extends along the end of the LiNbO_3 sample and contracts the upper H-guide plate. The hollow metal waveguide sections run straight through the device and are terminated by adjustable shorts for tuning. The bandwidth is restricted by the tuning elements, but the device is easy to construct and align.

Our device measurements were again made using the phase bridge technique described earlier. The insertion loss was 8 dB, of which 3 dB results from material absorption. We have not experimented with variation of the probe penetration depth into the metal waveguide (the penetration now is .030); optimum penetration could reduce the insertion loss below 8 dB. For a peak applied voltage of 1000 V, the amplitude modulation was 70%, and the induced phase shift was 58° peak-to-peak, in agreement with calculations.

B. Other Electro-optic Devices

1. Frequency Doublers

Materials which are useful for bulk phase shifting can also be used for nonlinear frequency doubling. The power conversion efficiency in this case can be written as

$$\frac{P(2\omega)}{P(\omega)} = \frac{2d^2 L^2}{\pi^3 c^3 \epsilon_0} \frac{P(\omega)}{A} \quad (\text{III-4})$$

where d is the microwave nonlinear coefficient, L is the interaction length, and A is the cross-sectional area. In writing Eq. III-4, we have assumed:

1. perfect phase matching
2. 100% mode confinement within the dielectric
3. negligible absorption.

If we assume that the length L is limited to α^{-1} , where α is the absorption coefficient, then the conversion efficiency in LiNbO_3 at 100 GHz is

$$\frac{P(2\omega)}{P(\omega)} = (9 \times 10^{-4}) \frac{P(\omega) (\text{kW})}{A (\text{mm}^2)} \quad (\text{III-5})$$

For an area of $0.5 \times 0.5 \text{ mm}^2$ and an input power of 10 kW (well below the dielectric breakdown threshold in LiNbO_3), the calculated efficiency is 3.6%. This will be reduced slightly when absorption is included in the calculation. The above conversion efficiency is already of practical interest, but still larger values are calculated for such materials as BaTiO_3 and KMnO_3 .

2. Electronically-scanned leaky-wave antennas

It is well known that periodically perturbed waveguides will radiate laterally at one or more fixed angles, thus leading to applications as scanning antennas. In fact, dielectric waveguides have been used for beam scanning via frequency sweeping [Ref. III-13]. Two disadvantages of this technique are that fixed frequency operation is not possible, and beam spread in the E-plane is large, since the waveguide height is small. In more recent work, Trinh et al. [Ref. III-14] eliminated the E-plane spreading by using an H-guide structure with flaring of the metal plates to produce a one-dimensional horn. Beam scanning was still obtained by frequency sweeping.

In both experiments described above, the dielectric guiding medium was silicon. If we substitute LiNbO_3 for the silicon, then the electro-optic properties of the LiNbO_3 can be used to provide scanning at a fixed frequency. Figure III-4 shows a sketch of the LiNbO_3 sample (with periodic indentations) and final H-guide antenna assembly. The lobe angle in the E-plane of the n th space harmonic is given by [Ref. III-13]:

$$\theta_n = \sin^{-1} \left[\frac{\lambda_0}{\lambda_g} + n \frac{\lambda_0}{d} \right] \quad (\text{III-6})$$

11473-16R1

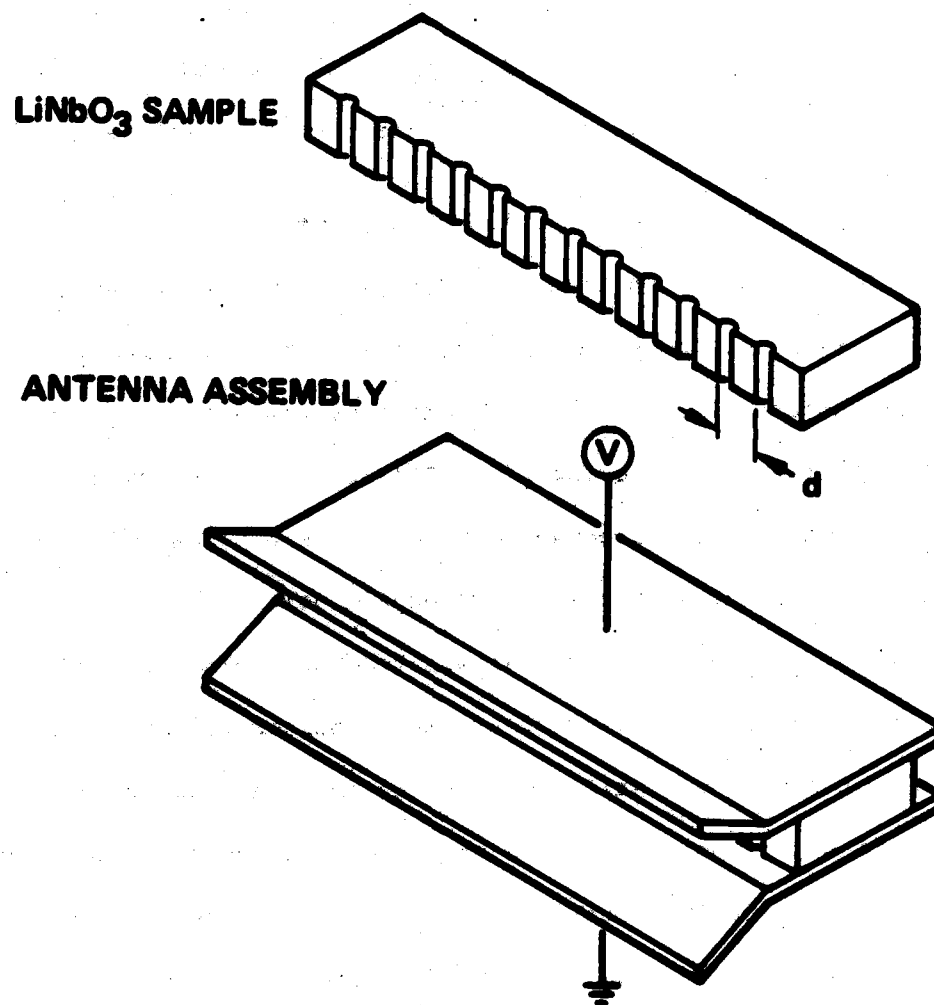


Figure III-4. Schematic representation of LiNbO₃ electronically scanned horn antenna.

where λ_0 is the free space wavelength, λ_g is the guide wavelength and d is the spacing between perturbations. In all cases of practical interest (with $\lambda_g < \lambda_0$) only negative values of m are possible. If we choose $d \approx \lambda_g$, then only the $m = -1$ harmonic will radiate so that

$$\theta_{-1} = \sin^{-1} \left[\frac{\lambda_0}{\lambda_g} - \frac{\lambda_0}{d} \right] \quad (\text{III-7})$$

By applying a modulating voltage between the two plates of the H-guide structure (Fig. III-4) λ_g can be varied, thus varying the angle θ_{-1} . If we assume that $\lambda_g = \lambda_0/n$, where n is the microwave refractive index, it is easy to show that the angular motion per unit of applied electric field (using $\Delta n = n^3 r \Delta E$) is:

$$\frac{\Delta \theta_{-1}}{\Delta E} = n^3 r \quad (\text{III-8})$$

where r is the electro-optic coefficient. Thus, the scanning antenna described here is characterized by the same figure of merit as the bulk phase modulator described earlier (see Eq. III-2). For a 20 kV/cm field in a LiNbO_3 device, $\Delta \theta_{-1} = \pm 0.6^\circ$. However, much larger scanning angles (on the order of 1 radian) are predicted for BaTiO_3 under the same conditions.

3. Electronically tunable filter

Fixed-frequency bandpass or bandstop filters have been demonstrated by coupling a pillbox or ring resonator to a wave travelling in dielectric waveguide. The center frequency in this type of device is determined by the dimensions and refractive index of the resonator structure. If the refractive index can be varied electro-optically, then the center frequency can be adjusted, resulting in a tunable filter. A sketch of such a device along with the output frequency spectrum is shown in Fig. III-5. The straight waveguide sections can be fabricated from a convenient low-loss material such as GaAs. The close-coupled ring resonator could be fabricated from

11473-21

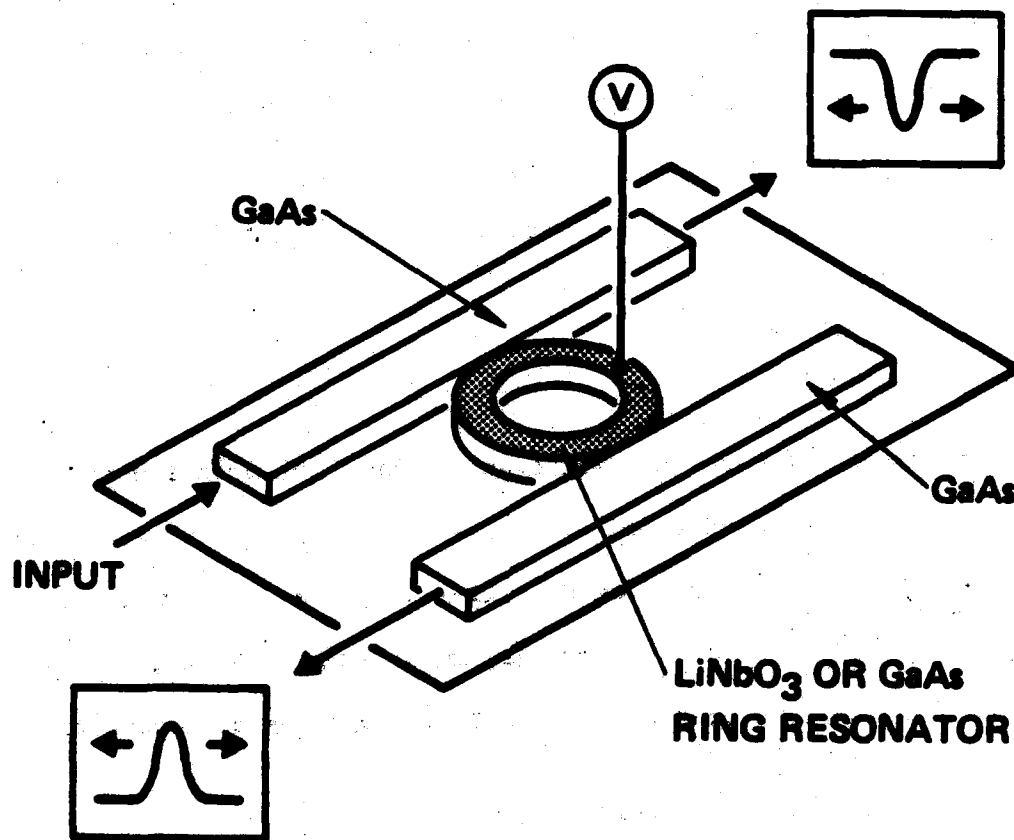


Figure III-5. Schematic representation of a tunable ring resonator filter based on image guide or H-guide. Both band-pass and band-reject characteristics can be realized.

LiNbO_3 (with a large electro-optic coefficient and moderate loss) or GaAs (with a smaller electro-optic coefficient and low loss).

To analyze this tunability of the device, we assume that the resonator Q (or linewidth) is determined by dielectric loss. The linewidth in this case is

$$\Delta\nu = \nu \tan\delta \quad . \quad (\text{III-9})$$

The center frequency ν can be written as

$$\nu = \frac{nc}{2n\pi D} \quad (\text{III-10})$$

where n is the order of interference, c is the speed of light, n is the refractive index and D is the ring diameter. The change in ν induced by a change in n is

$$\delta\nu = \frac{\Delta n}{n} \quad . \quad (\text{III-11})$$

Thus, the required index change to tune by one linewidth ($\delta\nu = \Delta\nu$) is obtained from combining Eqs. III-9 and III-11:

$$\Delta n = n \tan\delta \quad . \quad (\text{III-12})$$

Since $\Delta n = n^3 rE$, the field required to tune by one linewidth is

$$E = \frac{n \tan\delta}{(n^3 r)} = \frac{\tan\delta}{n^2 r} \quad . \quad (\text{III-13})$$

This field is equal to 20 kV/cm for LiNbO_3 , and 50 kV/cm for GaAs. We see that the tunability is limited, based on presently available materials. It is hoped that further reductions in dielectric loss at millimeter wavelengths will lead to improved filter performance.

F. Prospects for Improved Materials

It is clear from the previous discussion that there is a strong need for materials with large electro-optic/nonlinear coefficients and low losses.

The phase shifting performance of several candidate materials in their present state of development is plotted as a function of length in Fig. III-6. We have assumed an operating frequency of 94 GHz, and an applied field of 20 kV/cm. We note that certain materials with large electro-optic coefficients have low losses (e.g., GaAs), and perform nearly as well over a length $L \approx 1/\alpha$. The most promising material at present appears to be BaTiO_3 , although commercially available samples of this material are very expensive and of poor quality. Any materials improvements leading to lower absorption losses should lead to significantly improved device performance.

G. Conclusions and Future Plans

We have described the implementation of a number of electro-optic control devices in dielectric waveguide. The devices we describe still require the assembly and alignment of a number of carefully machined discrete components. An eventual goal would be the complete monolithic integration of all components onto a single chip.

At the present state of development, the most promising materials for device applications are LiNbO_3 , and perhaps GaAs. One important advantage of these materials is that they are readily available in large lengths (2-6 inches).

In the remaining year of this SRO Program, we plan to redesign the transitions in both H-guide phase shifter described in section D, in order to reduce the insertion loss. We also plan to construct and test a LiNbO_3 frequency doubler or scanning antenna using H-guide.

11473-22

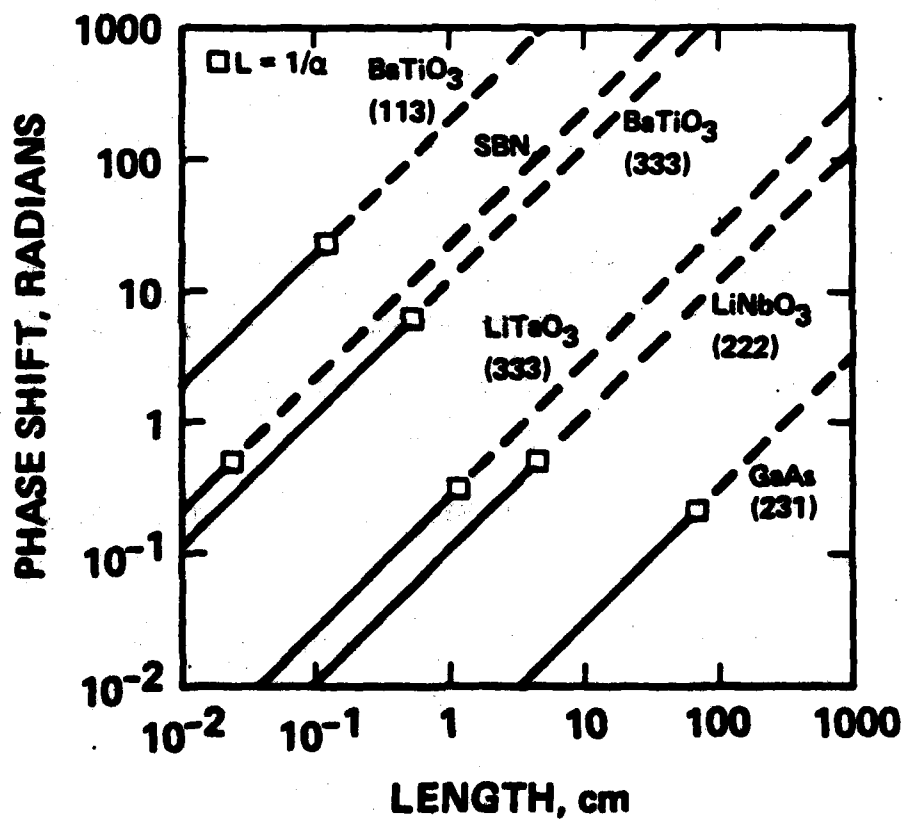


Figure III-6. Induced phase shift vs. length for several electro-optic materials and orientations. The box on each curve corresponds to the condition $L = 1/\alpha$, where α is the absorption coefficient for the given material and orientation.

REFERENCES FOR SECTION III

- III-1. B. J. Levin and G. G. Weidner, RCA Review, vol. 34, 1973, p. 489.
- III-2. H. Jacobs and M. M. Chrepta, IEEE Trans. Microwave Th. Tech., vol. MTT-22, 1974, p. 411.
- III-3. A. P. DeFonzo, Chi H. Lee and P. S. Mak, Appl. Phys. Lett., vol. 35, 1979, p. 575.
- III-4. Chi Lee and S. Mak, Elec. Lett. Vol. 14, 1978, p. 733.
- III-5. G. D. Boyd, T. J. Bridges, M. A. Pollack and E. H. Turner, Phys. Rev. Lett., vol. 26, 1971, p. 387.
- III-6. G. D. Boyd and M. A. Pollack, Phys. Rev., vol. B7, 1973, p. 5345.
- III-7. E. A. Vinogradov, N. A. Prisova and G. V. Kozlov, Sov. Phys. Solid State, vol. 12, 1970, p. 605.
- III-8. H. R. Fetterman, Chenming Hu, W. E. Barch and C. O. Parker, Lincoln Laboratory Quarterly Technical Summary Report, June 1975, p. 30.
- III-9. M. B. Klein, Int. J. Infrared and Millimeter Waves, vol. 2, 1981, p. 239.
- III-10. F. J. Tischer, Proc, Inst. Elec. Eng., vol. 106B, Suppl. 13, 1959, p. 47.
- III-11. M. Cohn, IRE Trans. Microwave Th. Tech., vol. MTT-7, 1959, p. 202.
- III-12. M. Cohn and F. F. Eikenberg, IRE Trans. Microwave Th. Tech., vol. MTT-10, 1962, p. 36.
- III-13. K. L. Klohn, R. E. Horn, H. Jacobs and E. Freibergs, IEEE Trans. Microwave Th. Tech., vol. MTT-26, 1978, p. 764.
- III-14. T. N. Trinh, R. Mittra and R. J. Paleta, "Horn Image Guide Leaky-Wave Antenna," Proc. of Intl. Microwave Symp., Los Angeles, November 1981.

DISTRIBUTION LIST - TECHNICAL REPORTS
Contract N00014-79-C-0839

Office of Naval Research Code 427 Arlington, VA 22217	4	Dr. H. C. Nathanson Westinghouse Research and Development Center Beulah Road Pittsburgh, PA 15235	1
Naval Research Laboratory 4555 Overlook Avenue, S.W. Washington, D.C. 20375 Attn: Code 6811 6850	1 1	Dr. Daniel Chen Rockwell International Science Center P.O. Box 1085 Thousand Oaks, CA 91360	1
Defense Logistics Agency Defense Documentation Center Bldg. 5, Cameron Station Alexandria, VA 22314	12	Dr. D. Krumm Hughes Research Laboratory 3011 Malibu Canyon Road Malibu, CA 90265	
Dr. Y. S. Park AFWAL/DHR Building 450 Wright-Patterson AFB Ohio 45433	1	Mr. Lothar Wandinger ECOM/AMSEL/TL/LJ Forth Monmouth, NJ 07003	1
ERADCOM DELET-M Fort Monmouth, NJ 07703	1	Dr. Harry Wieder Naval Ocean Systems Center Code 922 271 Catalina Blvd. San Diego, CA 92157	1
Texas Instruments, Inc. Central Research Lab. M.S. 134, P.O. Box 225936 13500 North Central Expressway Dallas, TX 75265 Attn: Dr. Wisseman	1	Dr. William Lindley MIT Lincoln Laboratory F124 A, P.O. Box 73 Lexington, MA 02173	1
Dr. R. M. Malbon/M.S. IC Avantek, Inc. 3175 Bowers Avenue Santa Clara, CA 94304	1	Commander U.S. Army Electronics Command V. Gelnovatch (DRSEL-TL-IC) Fort Monmouth, NJ 07703	1
M. R. Bierig Raytheon Company 28 Seyon Street Waltham, MA 02154	1	RCA Microwave Technology Center Dr. F. Starzer Princeton, NJ 08540	1
Dr. R. Bell, K-101 Varian Associates, Inc. 611 Hansen Way Palo Alto, CA 94304	1	Watkins-Johnson Company E.J. Crescenzi, Jr./K. Niclas 3333 Hillview Avenue Stanford Industrial Park Palo Alto, CA 94304	1
Hewlett-Packard Corp. Dr. Robert Arthur 1501 Page Mill Road Palo Alto, CA 94306	1		

Distribution List - Technical Reports (continued)

Commandant Marine Corps Scientific Advisor (Code AX) Washington, D.C. 20380	1	AIL TECH 612 N. Mary Avenue Sunnyvale, CA 94086 Attn: G. D. Vendelin	1
Communications Transistor Corporation Dr. W. Waisenberg 301 Industrial Way San Carlos, CA 94070	1	Professors Hauser and Littlejohn Department of Electrical Engineering North Carolina State Univ. Raleigh, NC 27607	1
Microwave Associates Northwest Industrial Park Drs. F. A. Brand/J. Saloom Burlington, MA 01803	1	Professor J. Beyer University of Wisconsin- Madison 750 University Avenue Madison, Wisconsin 53706	1
Commander, AFAL AFWAL/AADM Dr. Don Rees Wright-Patterson AFB Ohio 45433	1	General Electric Company Attn: W. Perkins Electronics Lab 3-115/B4 P.O. Box 4840 Syracuse, NY 13221	1
Professor Walter Ku Phillips Hall Cornell University Ithaca, NY 14853	1	Professors Rosenbaum and Wolfe Washington University Semiconductor Research Lab. P.O. Box 1127 St. Louis, Missouri 63130	1
Commander Harry Diamond Laboratories Mr. Horst W. A. Gerlach 2800 Powder Mill Road Adelphia, MD 20783	1	Mr. John Carson Code 8212 NOSC San Diego, CA 92152	1
Advisory Group on Electron Devices 201 Varick Street 9th Floor New York, NY 10014	1	Dr. Hans Steyskal RADC/EEA Hanscom AFB, MA 01731	1
D. Claxton MS/1414 One Space Park Redondo Beach, CA 90278	1	Dr. Richard Brandt ONR WEST 1030 E. Green Street Pasadena, CA 91106	2
Professor L. Eastman Phillips Hall Cornell University Ithaca, NY 14853	1	Professor Donald M. Bolla Dept. of Electrical and Computer Engineering Lehigh University Bethlehem, PA 18015	1